MATISSE

Barcelonnette school, Sept. 2013,

Bruno Lopez, Stéphane Lagarde and the project Consortium

Descartes and Swedenborg,
17th and first part of the 18th centurie.

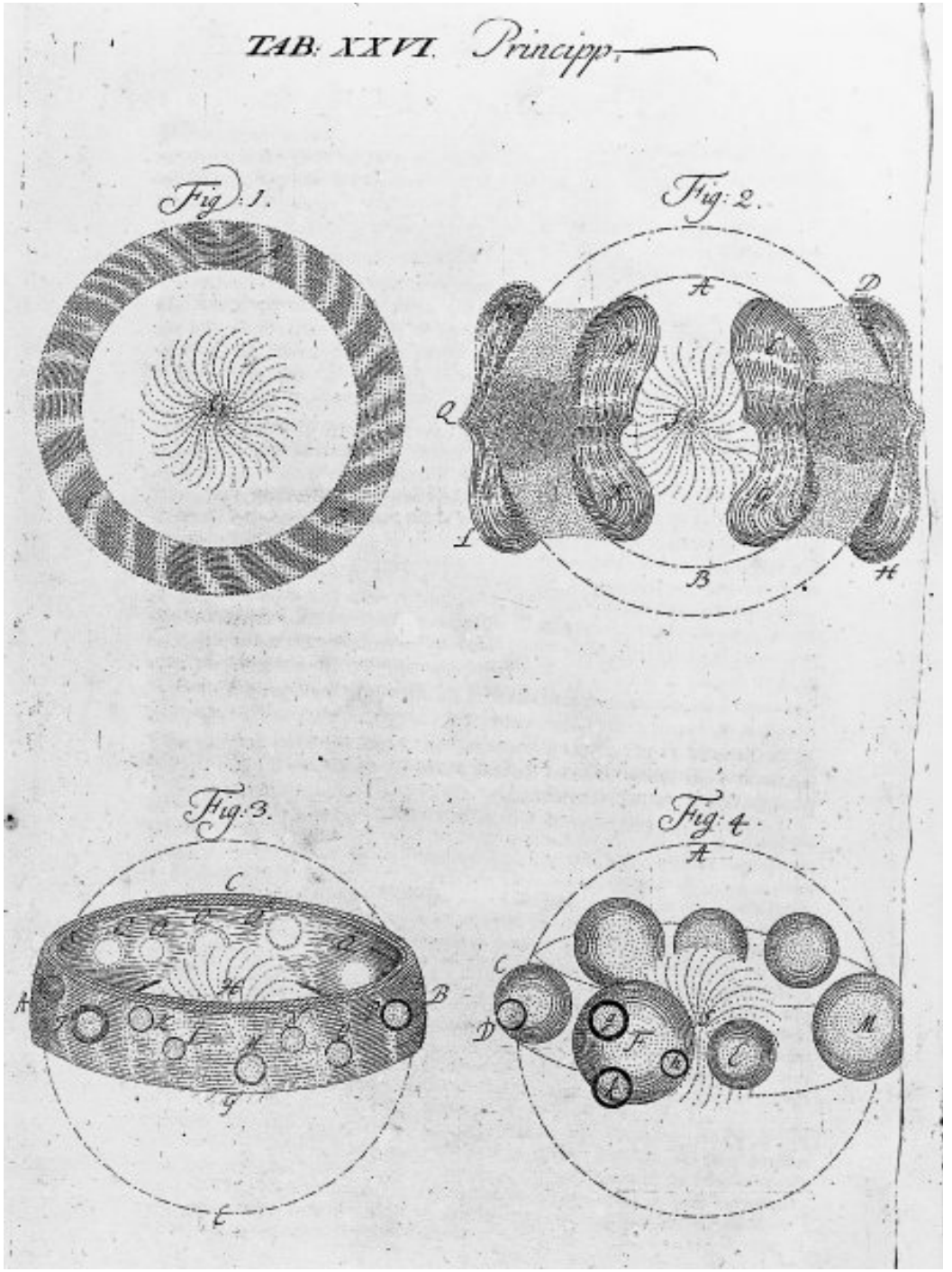

The protosolar nebula of Kant (1724-1804) & Laplace (1749-1827)

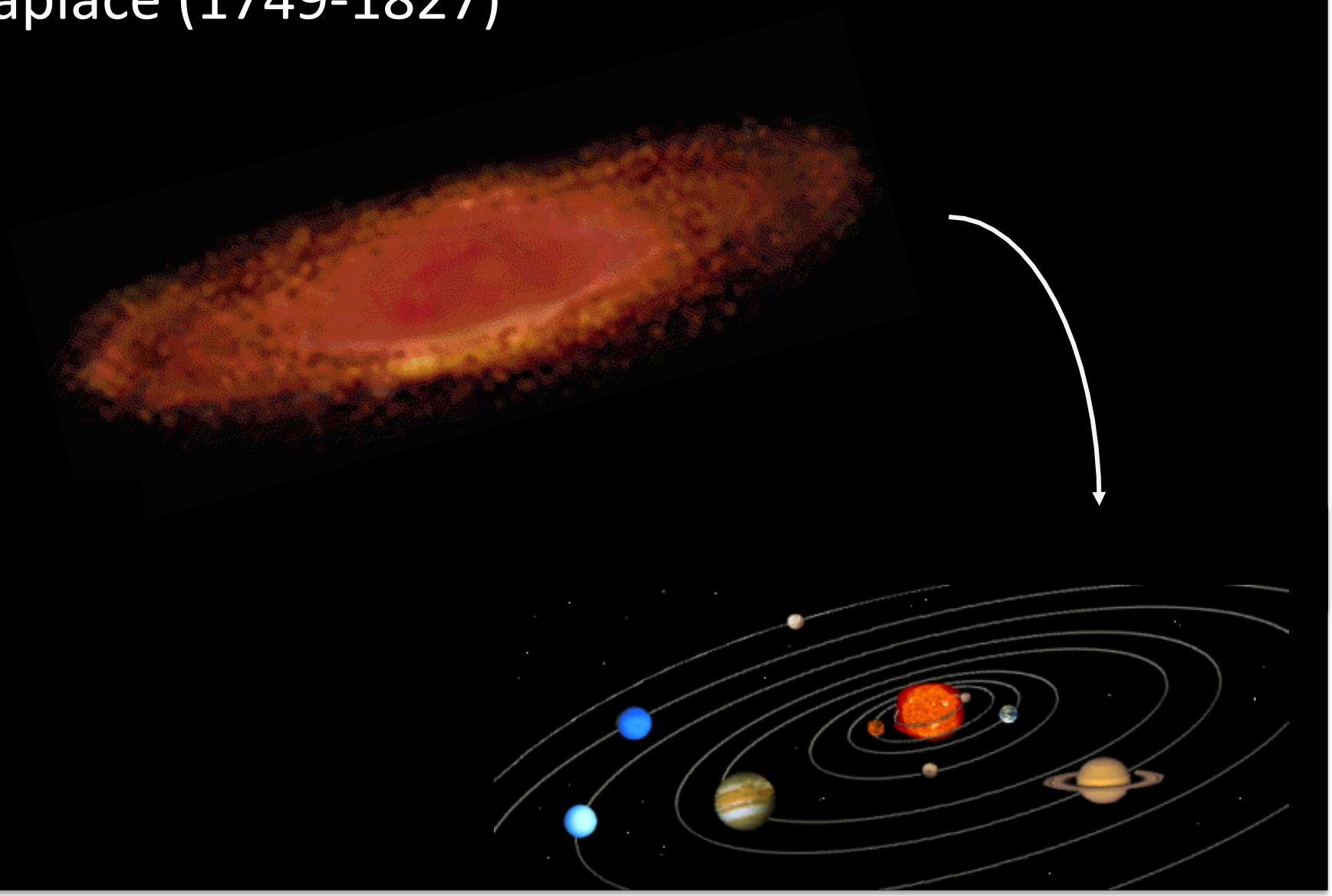

Known at the Kant and Laplace epoch

- Planets : Mercure, Venus, Mars, Jupiter, Saturne, (1781) Uranus, (1847) Neptune.
- Galilée refractor (1609) et Newton telescope (1668).
- Kepler planet orbits (1571-1630).
- Messier planetary nebulae catalogue. Charles Messier, 1730-1817.

Not known : the galaxies : Hubble 1889-1953.

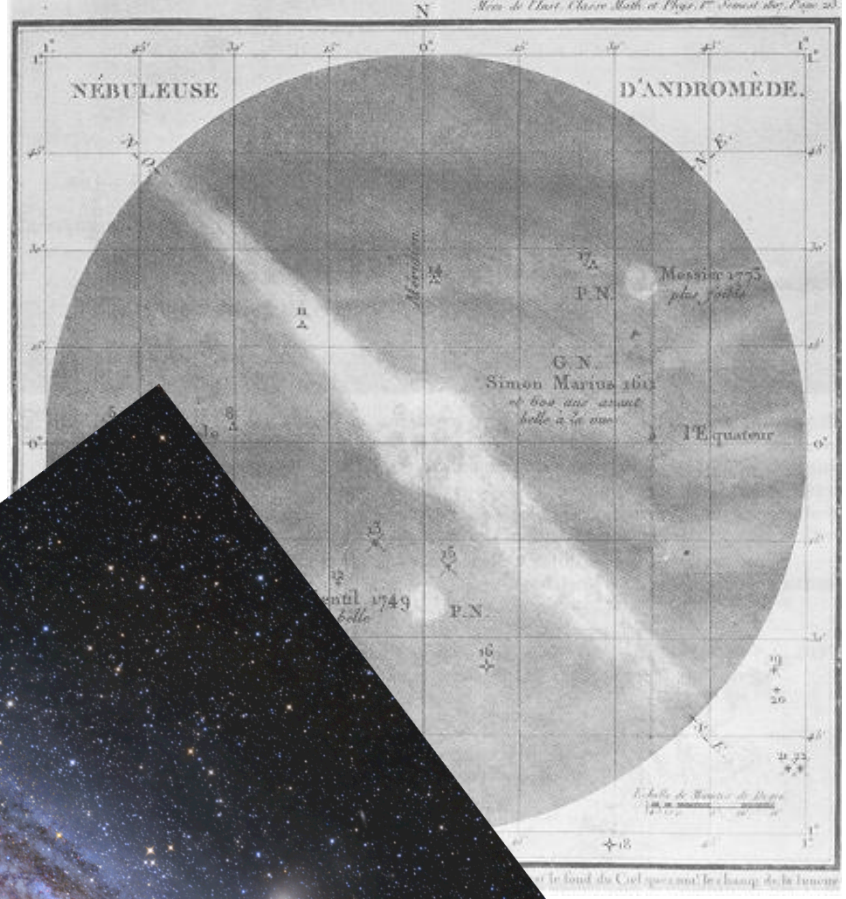
NÉBULEUSE
D'ANDROMÈDE.
Messier 1755
plus petite
P.N.
G.N.
Simon Marius 1612
l'Equateur
P.N.

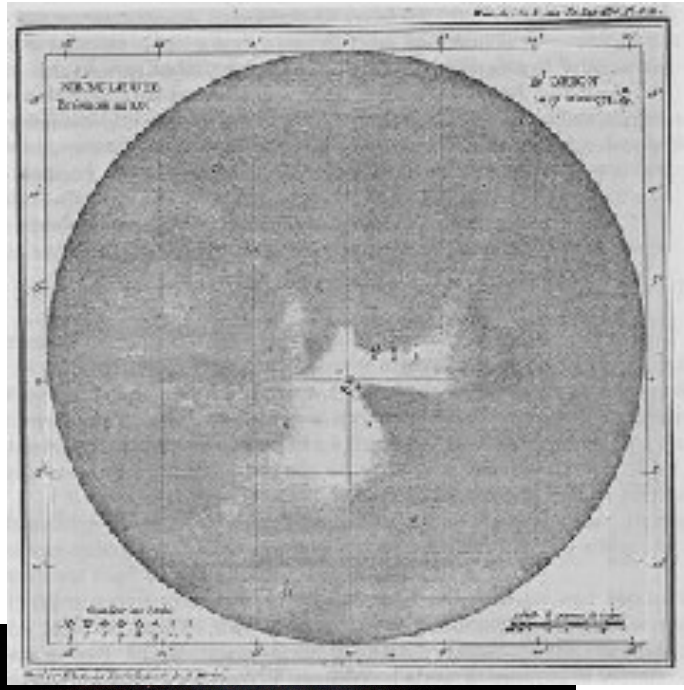

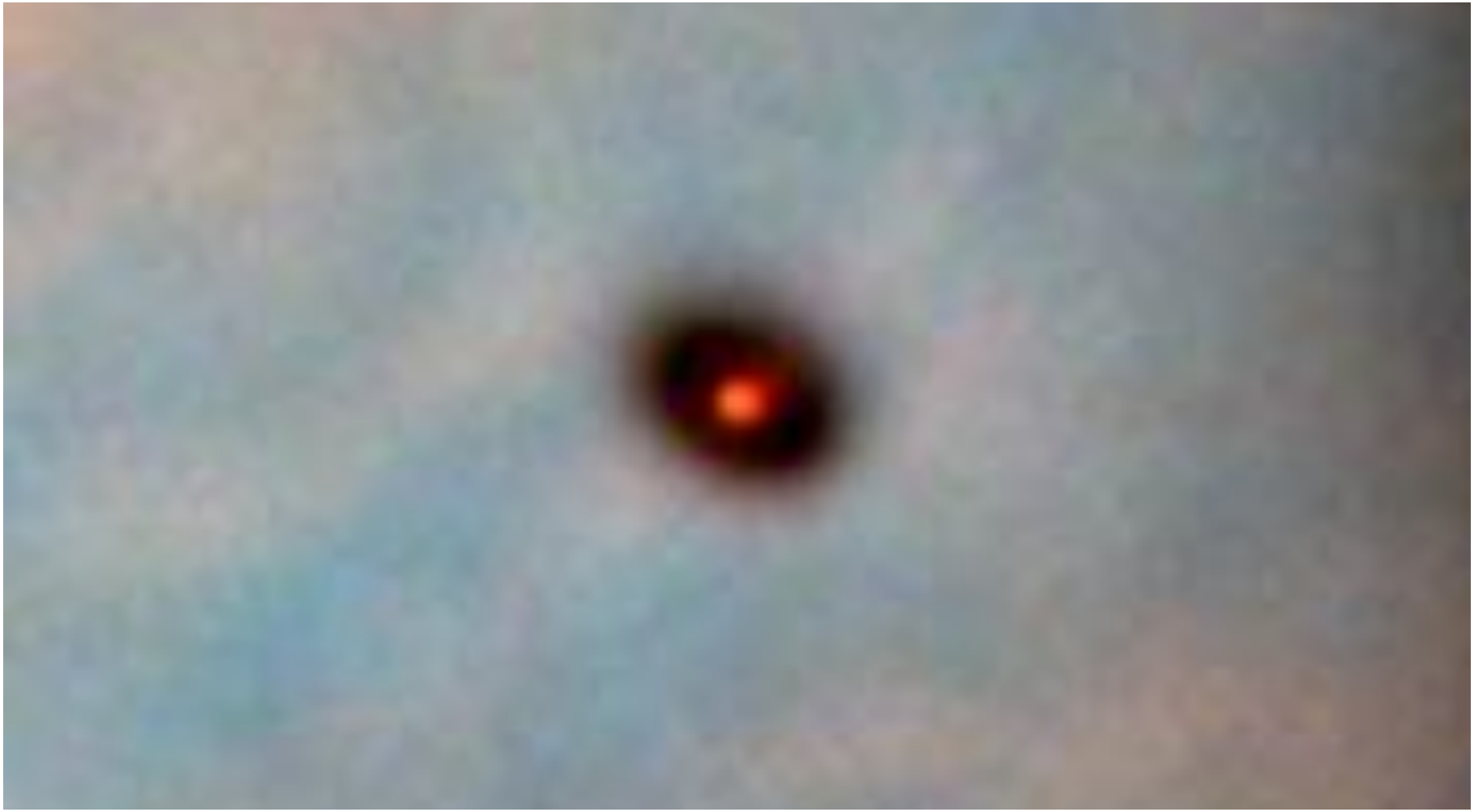

How the planets form and evolve, requires the understanding of protoplanetary disks

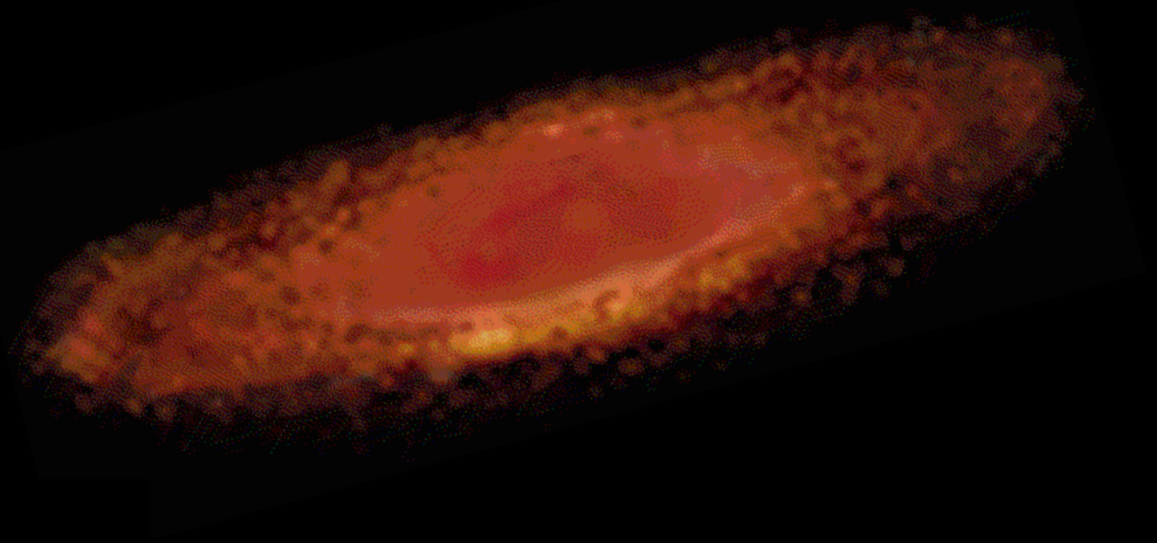

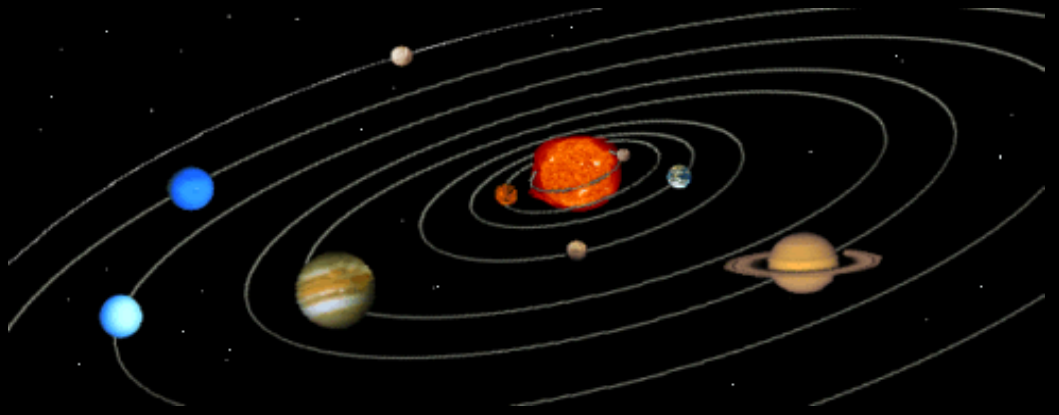

How the planets form and evolve, requires the understanding of protoplanetary disks

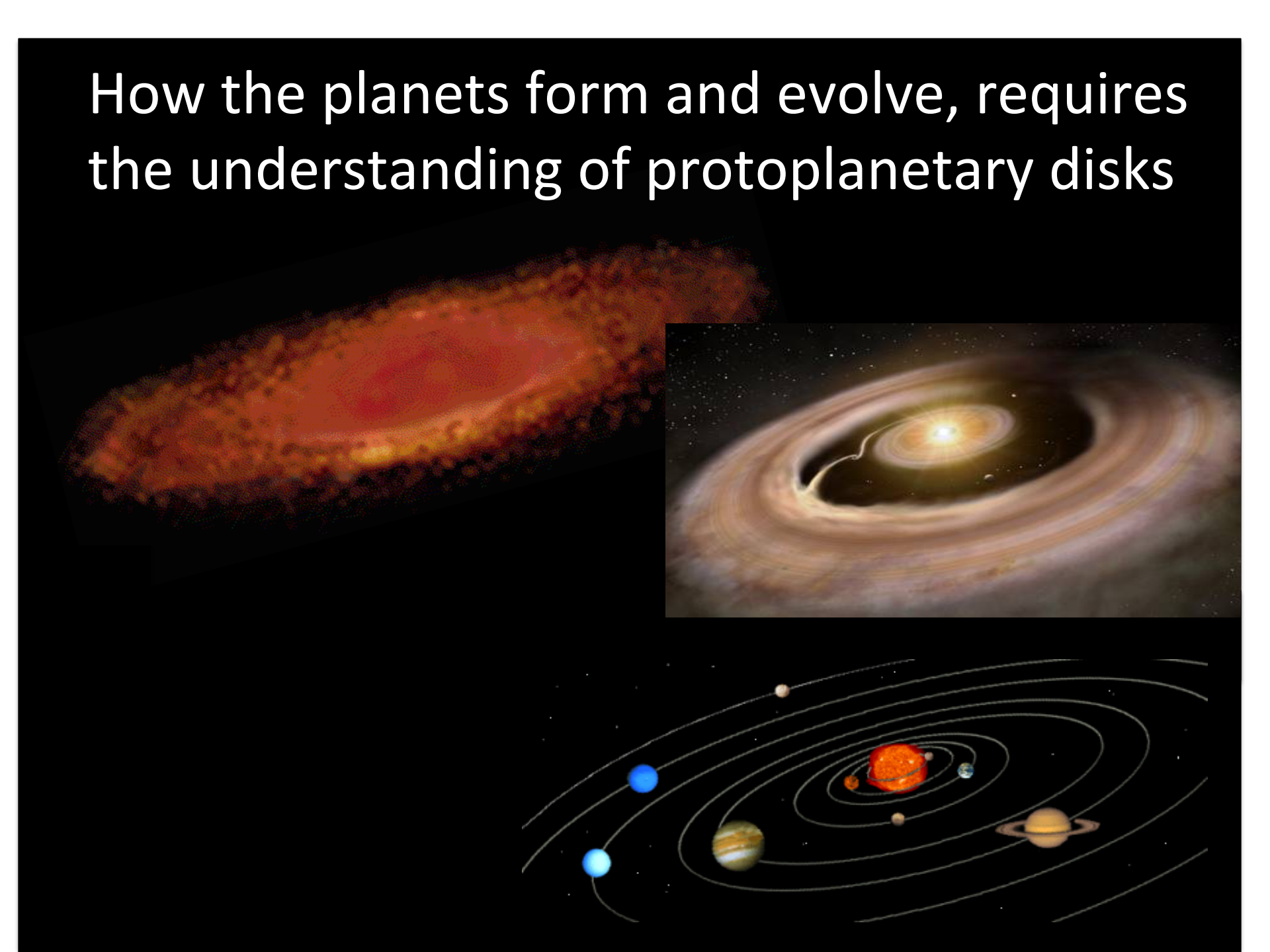

The potential of optical interferometry and the use of the mid-infrared domain.

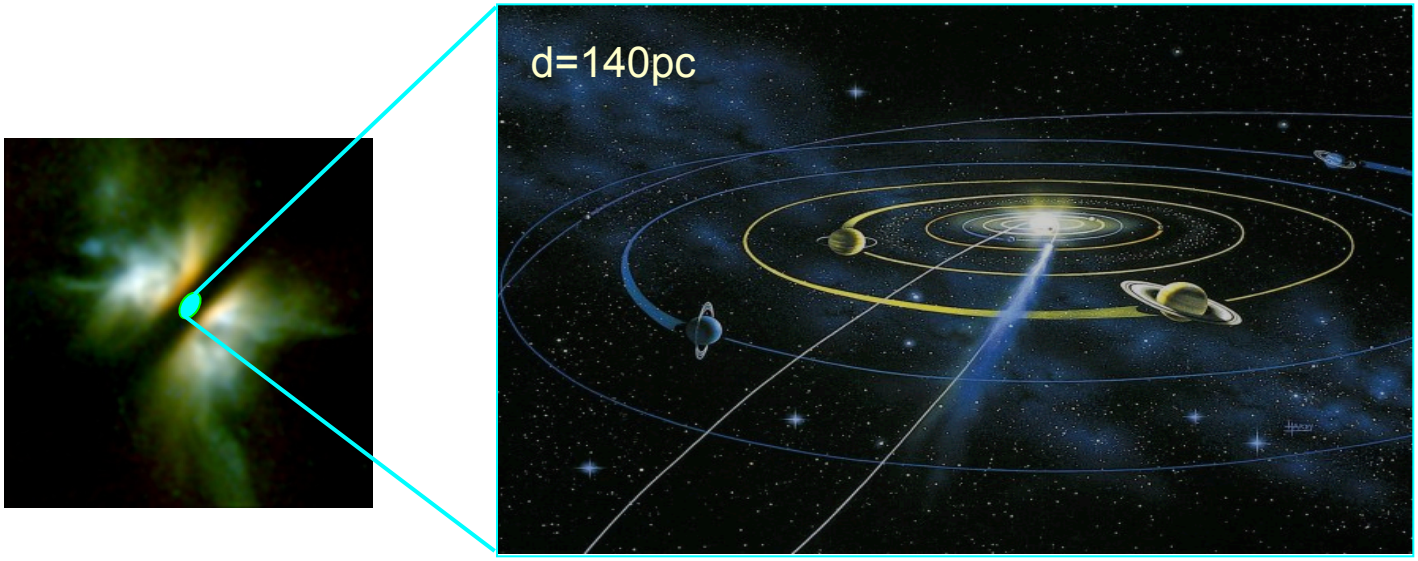

Angular distance Earth-Sun at 140 parsecs = 7 milli-seconds of arc (7mas).

… Jupiter-Sun = 36 mas

… Neptune-Sun = 215 mas


Carina-Sagittarius Arm
Norma Ar
10 000
20 000
Perseus Arm
<- Our Solar System
30 000
Local or Orion Arm

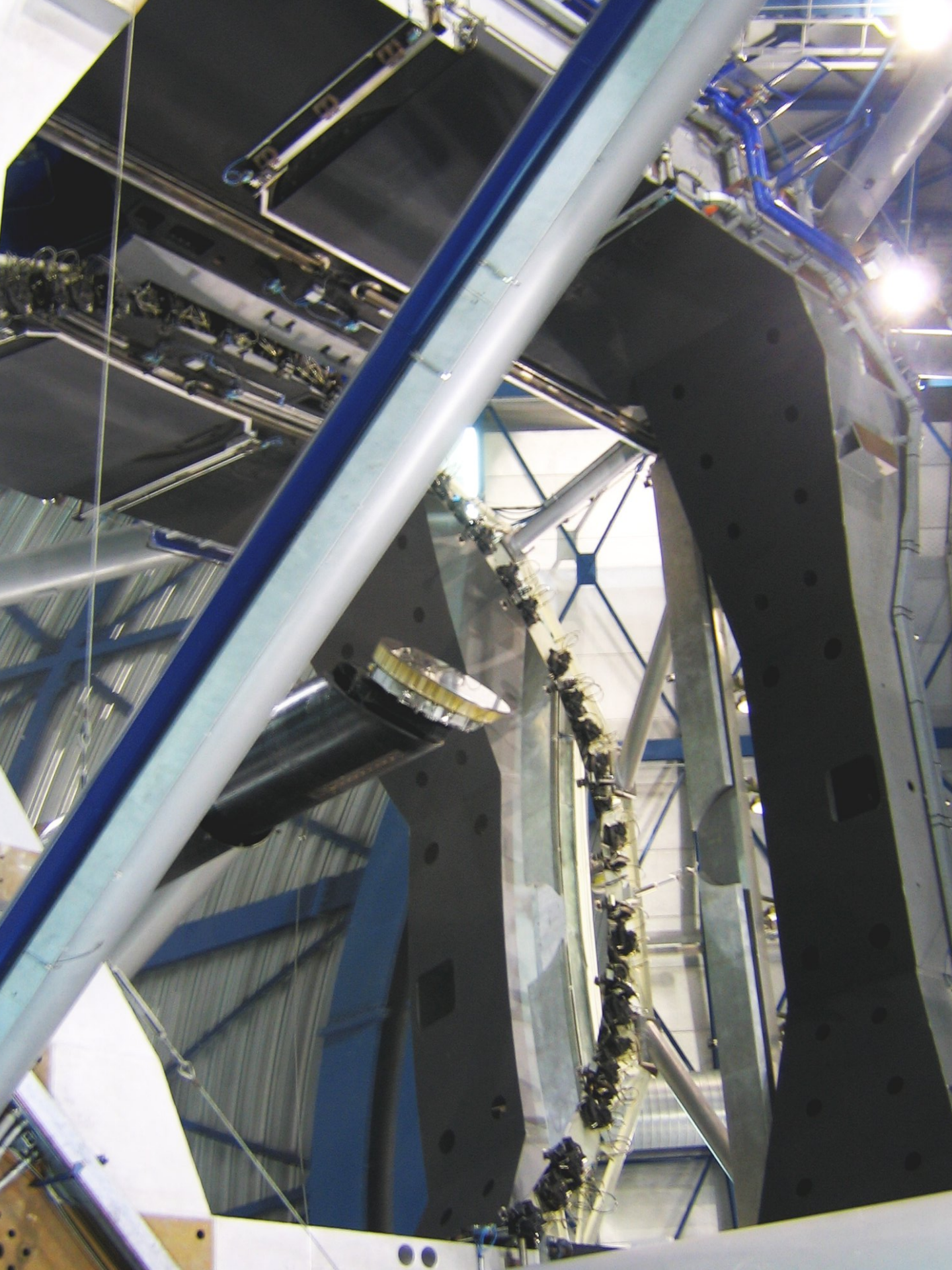

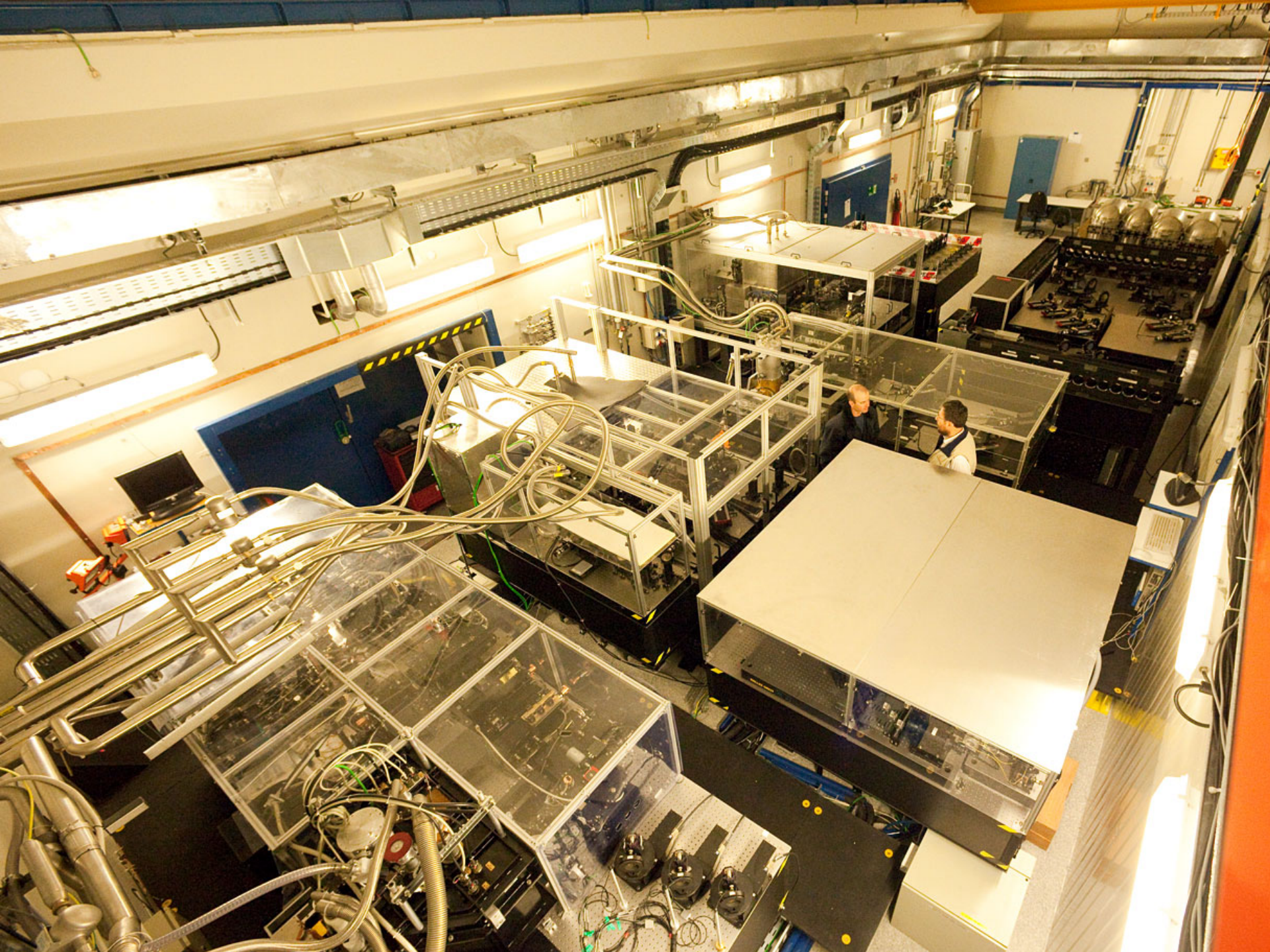


2
1


Intermède musical

The ‘Trophée des Alpes’ seen by a telescope of 100 meter diameter at 2000 kilometers.

Fourier Transform

TF^{-1}

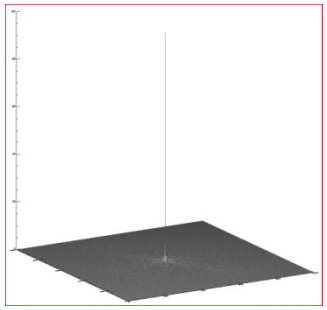

Real part

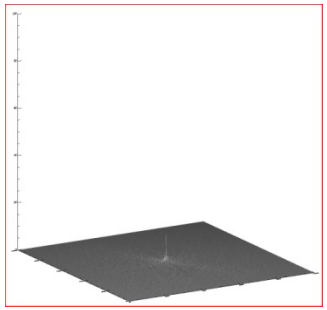

Imaginary part

Filter :
‘the modulation transfer function’

X

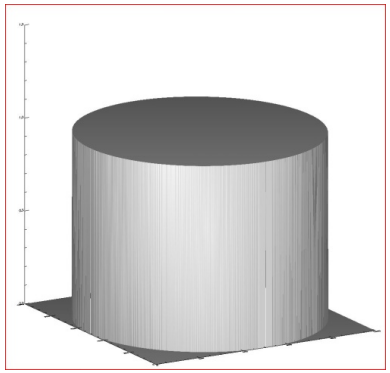

=

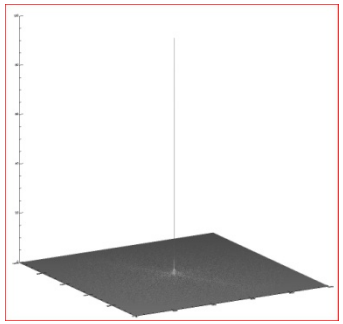

Real filtered

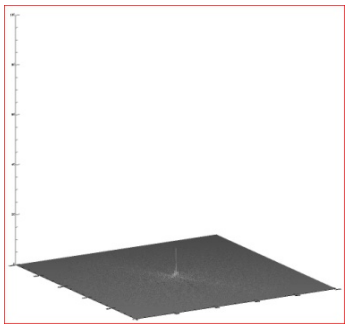

Imaginary filtered

A 10 m telescope diameter

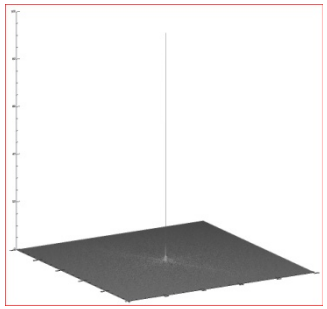

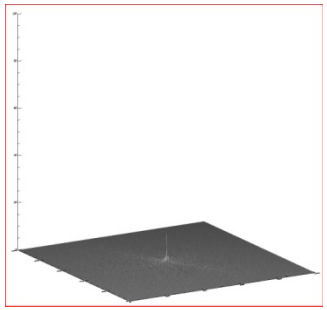

X

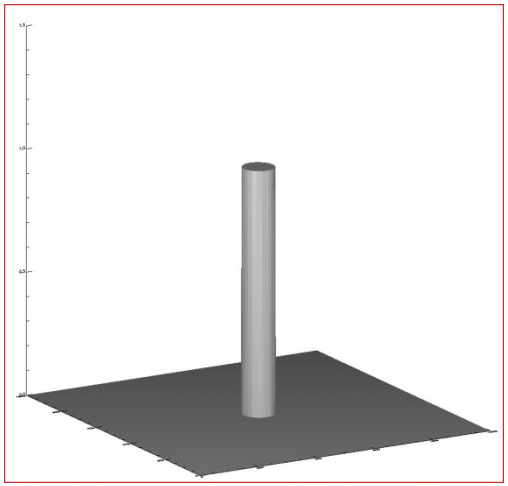

=

TF^{-1}

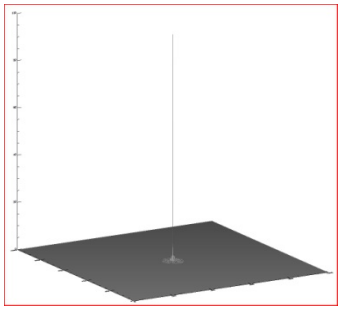

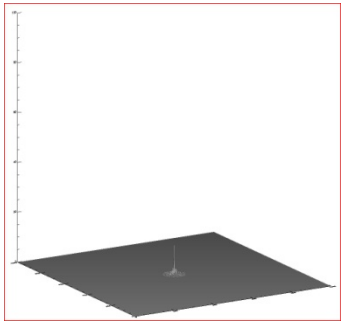

A 2 meter telescope

TF

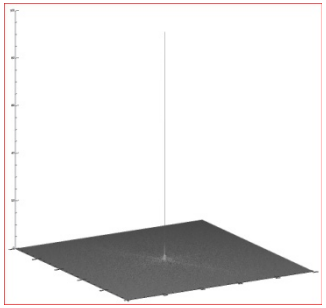

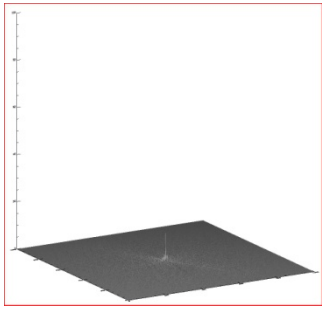

X

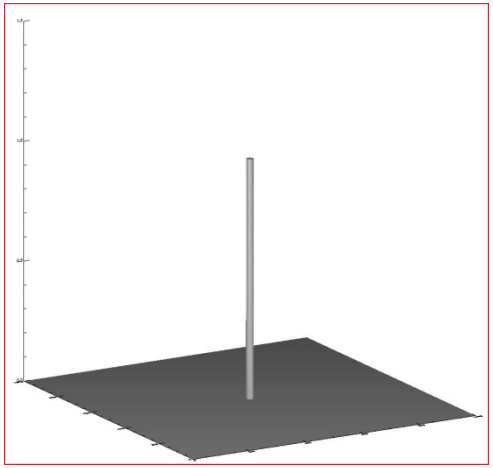

=

TF^{-1}

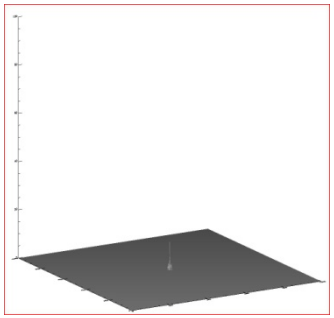

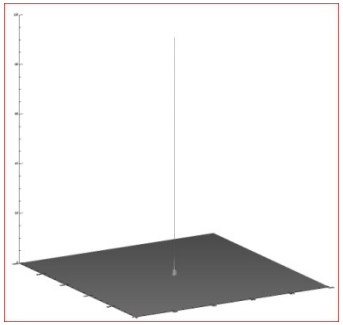

Annular filter

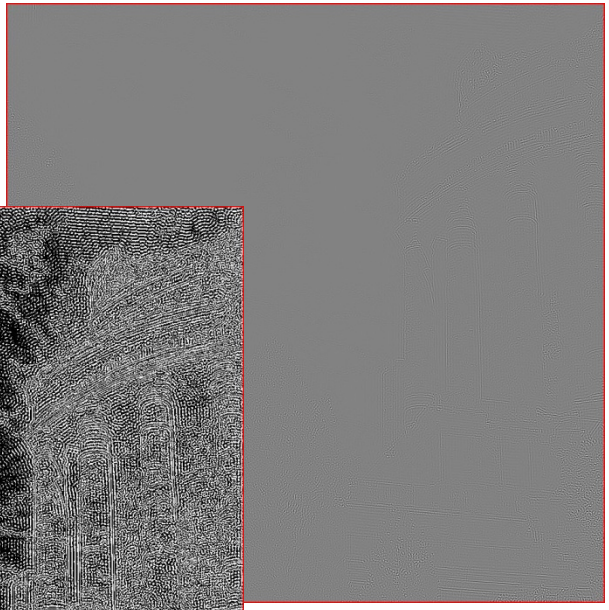

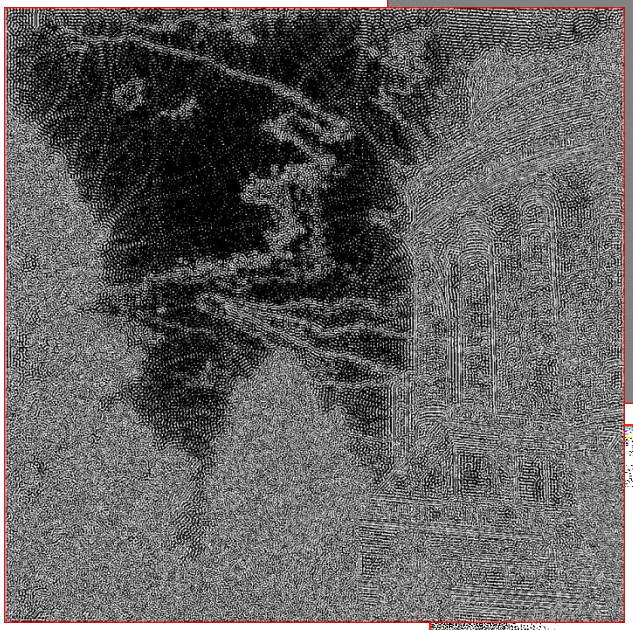

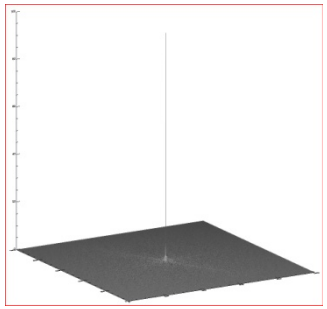

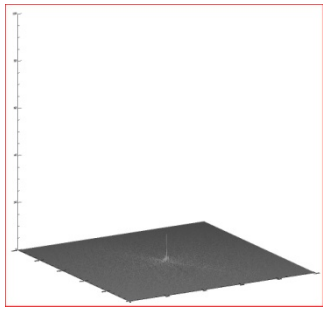

X

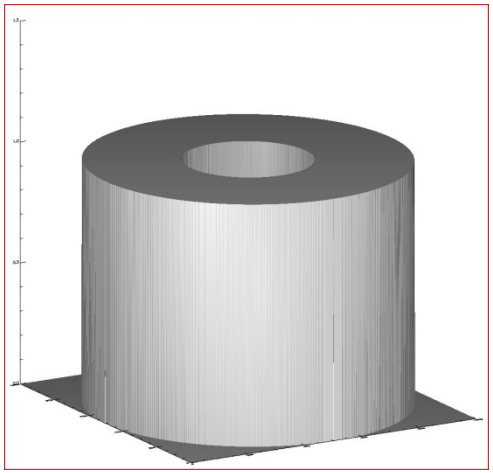

=

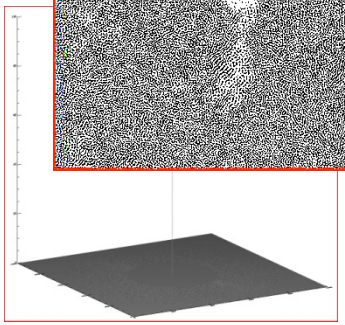

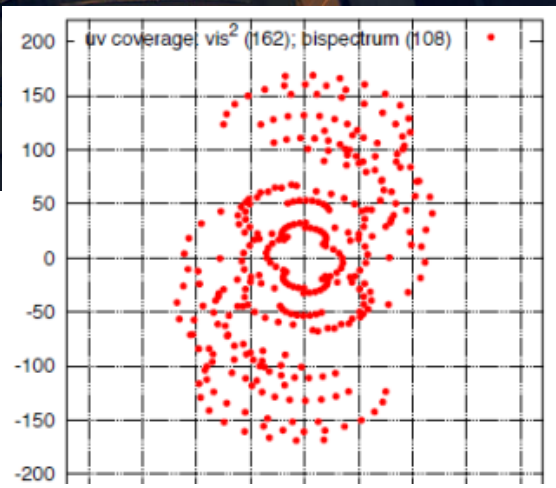
uv coverage; vis^2 (162); bispectrum (108)
200
150
100
50
0
-50
-100
-150
-200

An interferometer composed of 2 meter telescopes

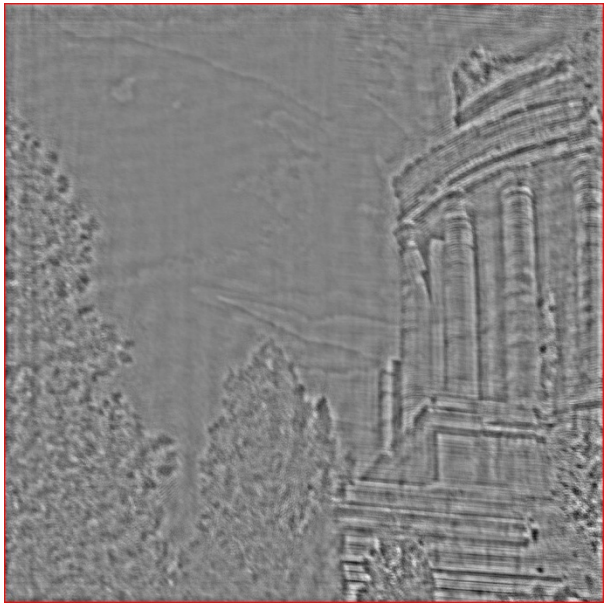

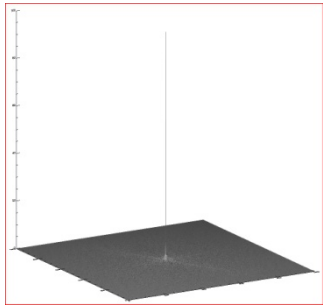

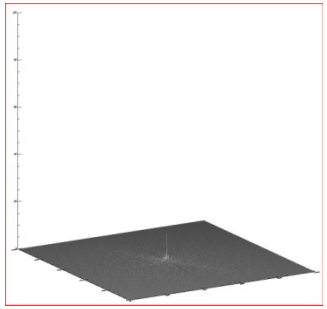

X

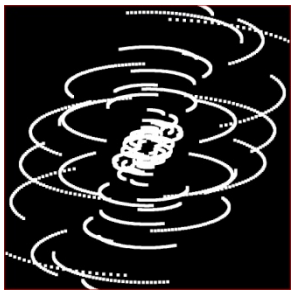

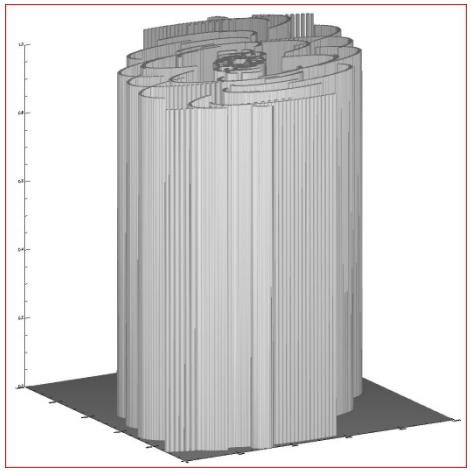

=

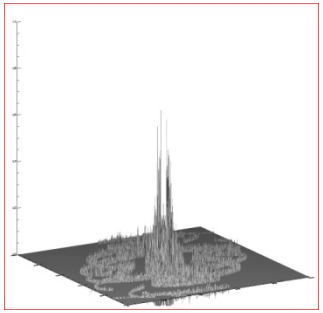

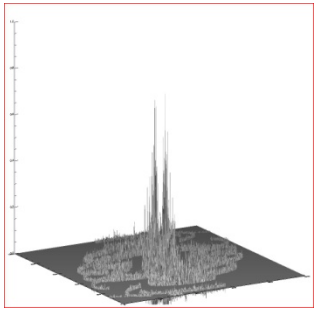

TF^{-1}

An interferometer of 2 m class telescopes + a 10 meter diameter telescope.

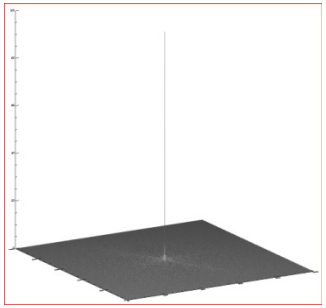

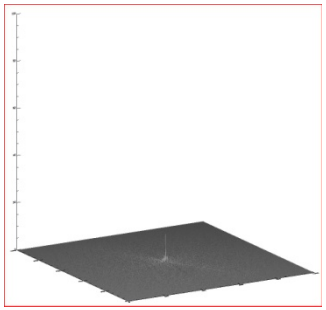

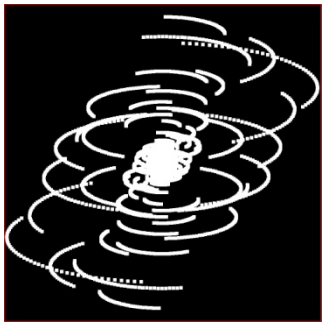

TF^{-1}

X

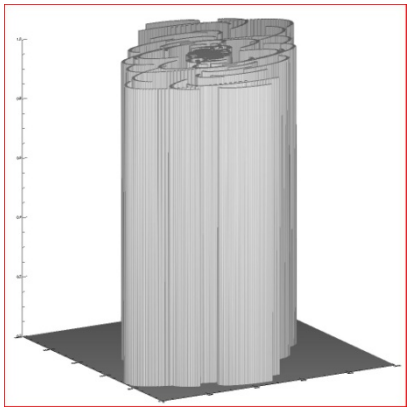

=

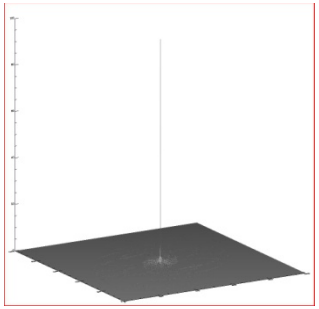

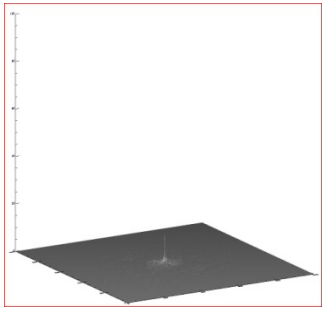

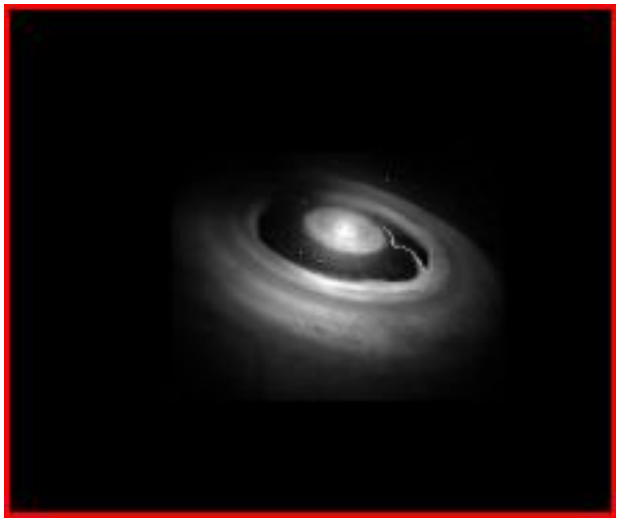

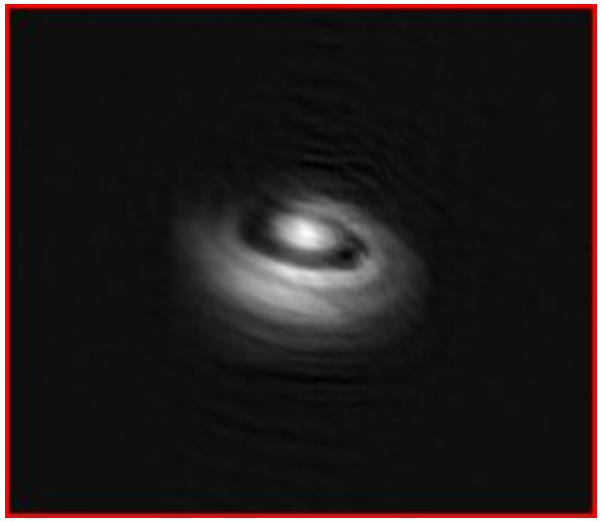

TF

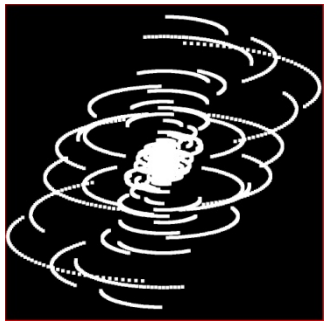

TF^{-1}

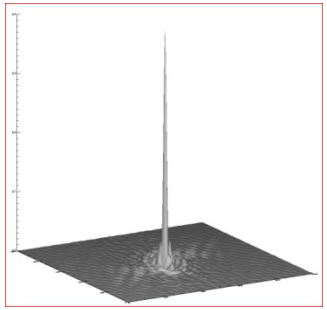

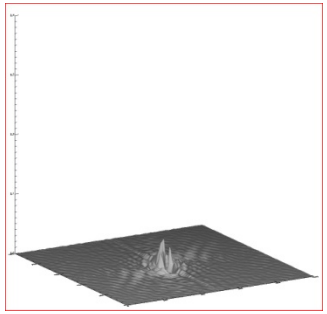

X

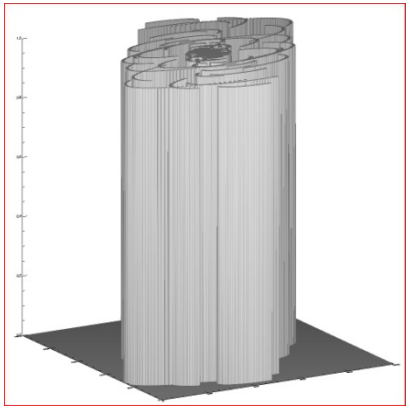

=

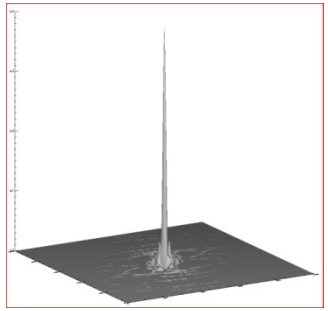

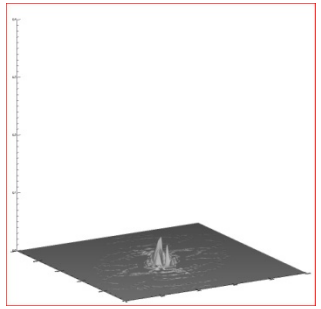

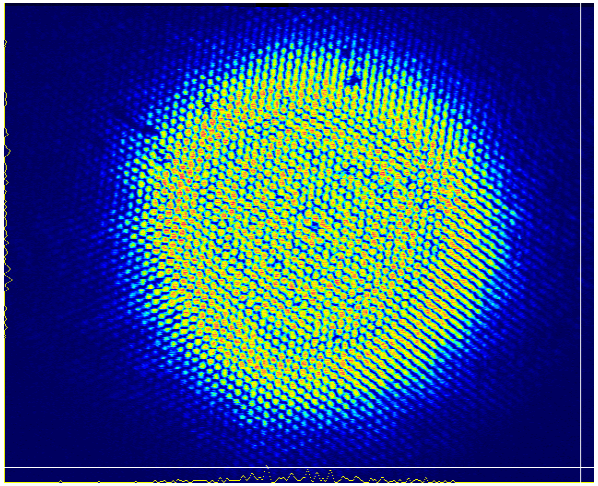

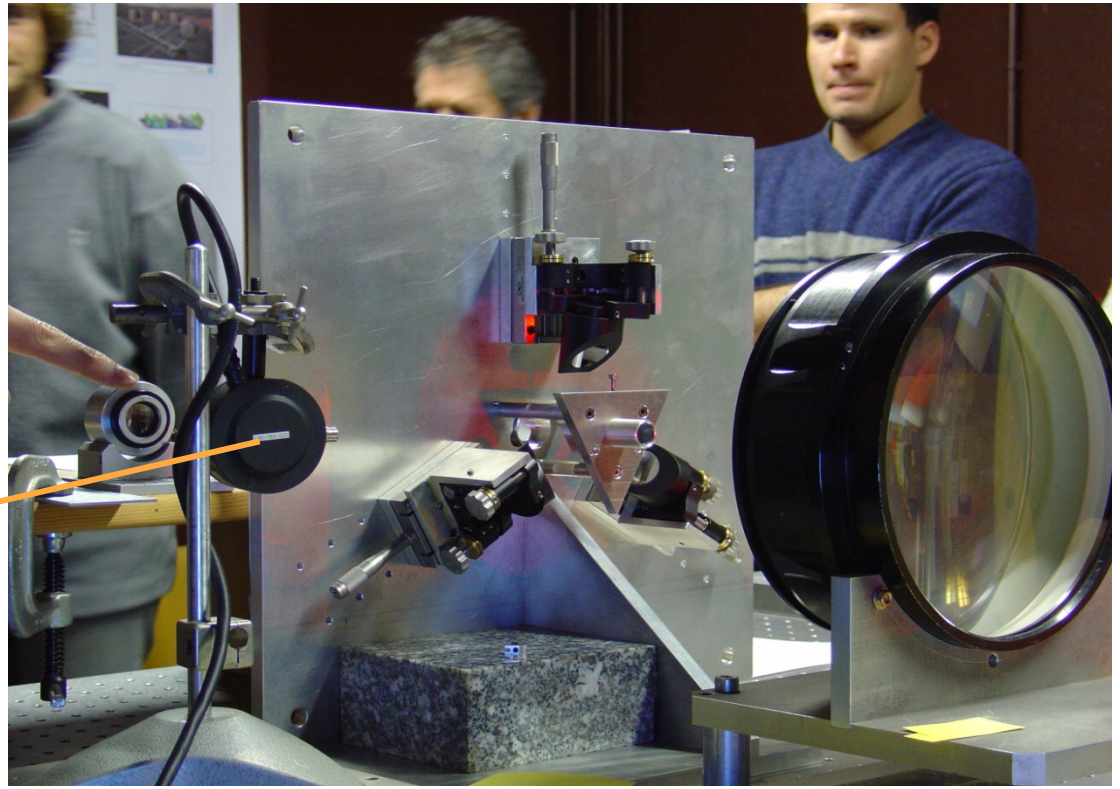

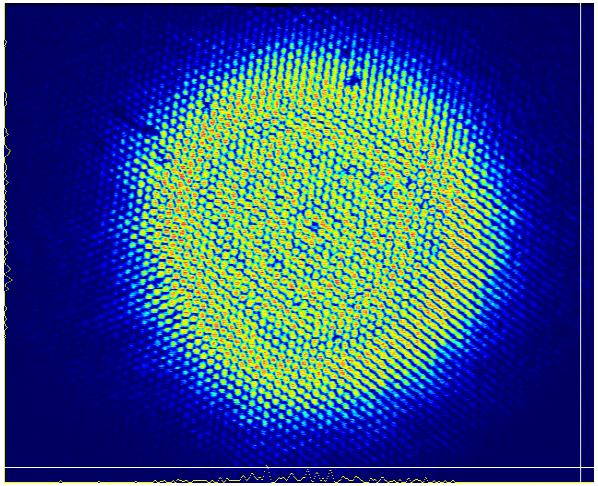

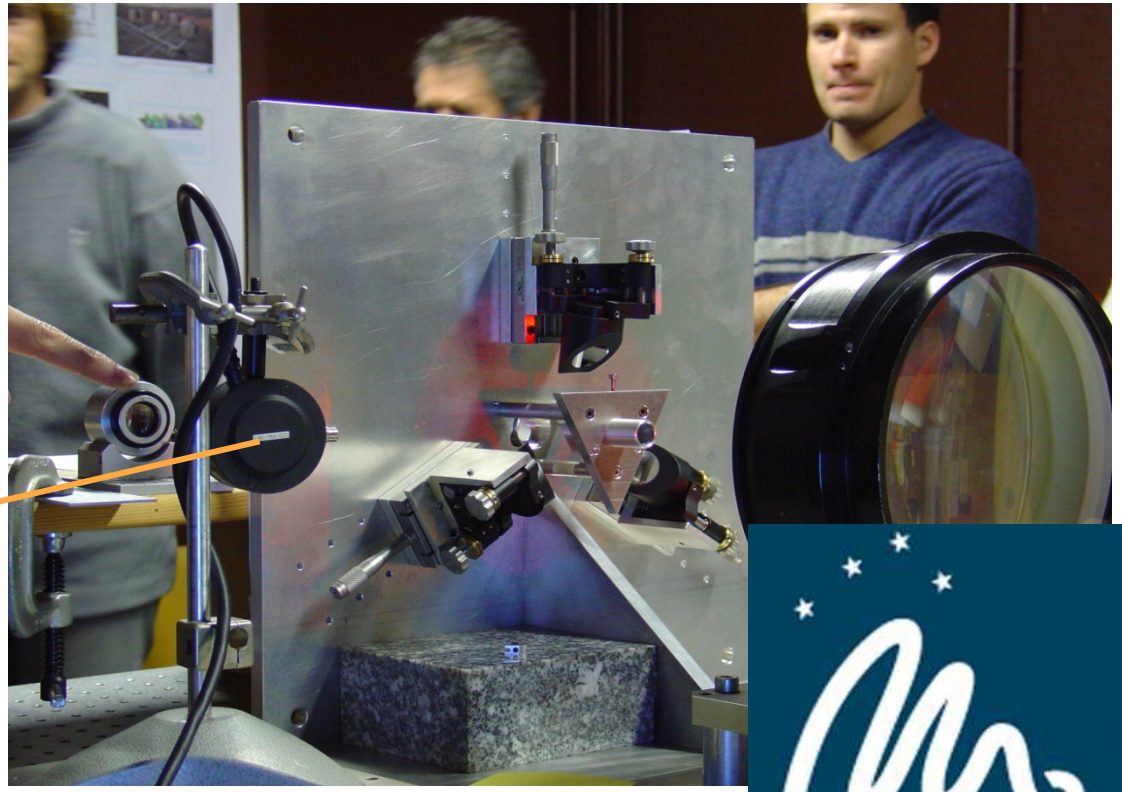

MATISSE

Concept of the instrument

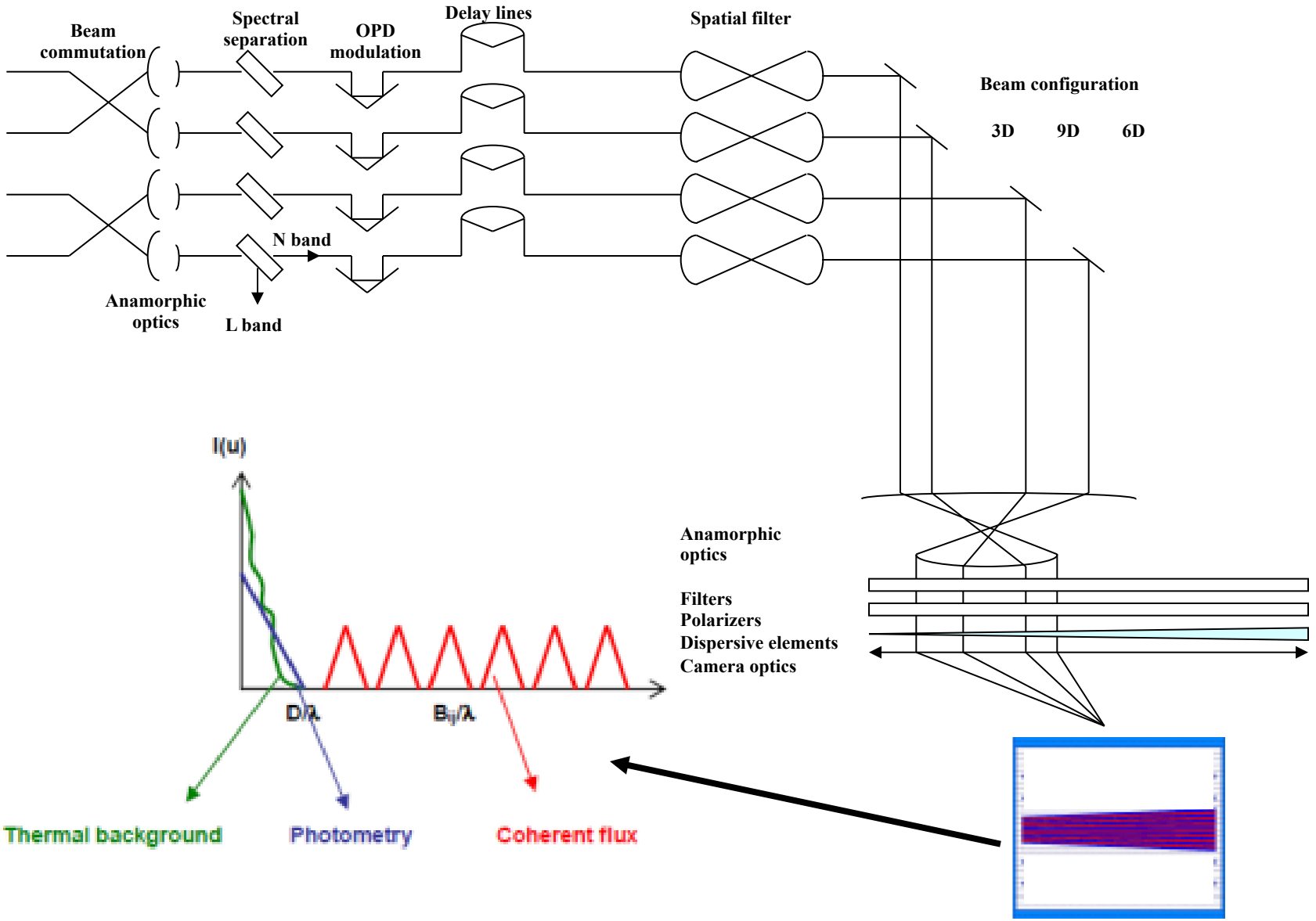

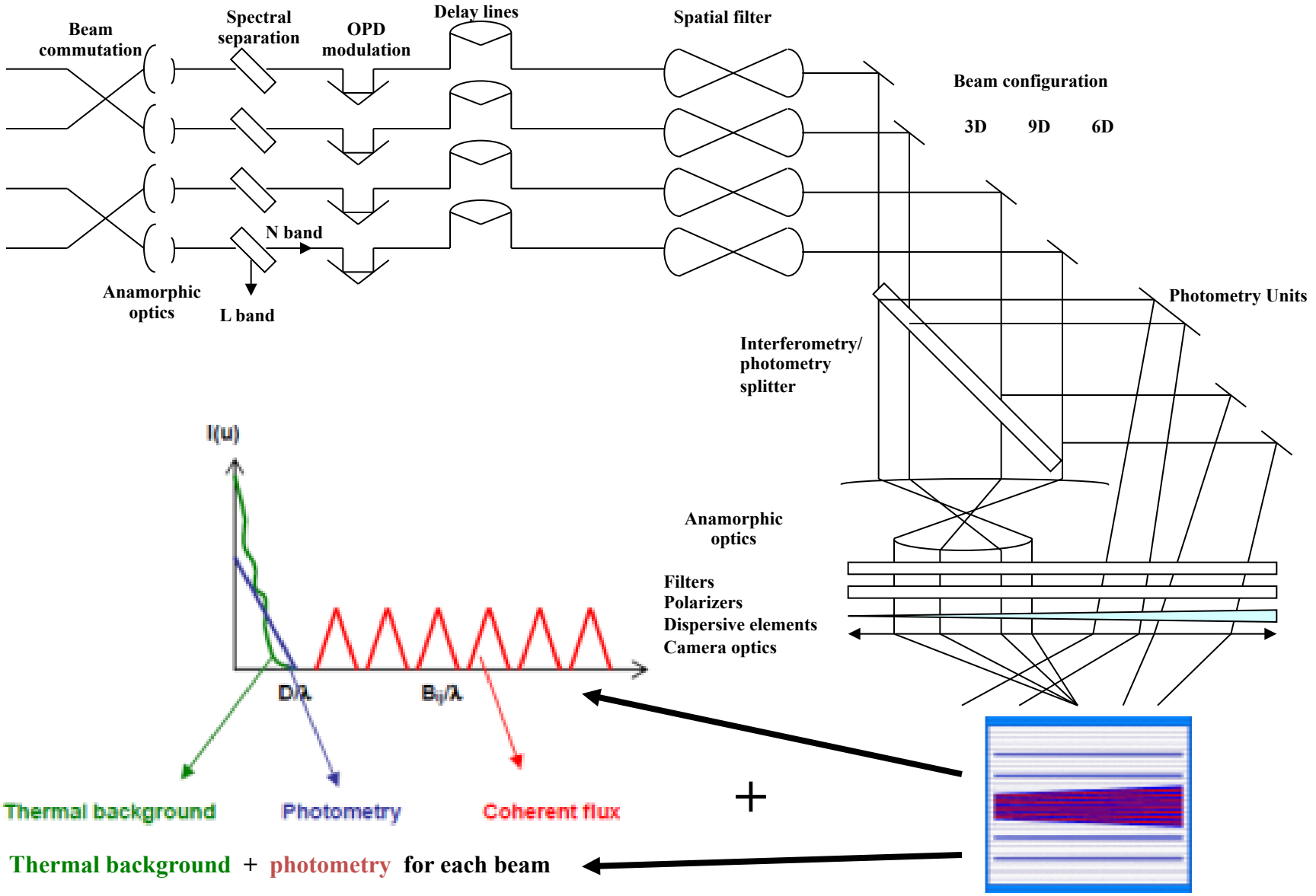
Beam commutation
Spectral separation
OPD modulation
Delay lines
Spatial filter
Beam configuration
3D
9D
6D
N band
Anamorphic optics
L band
Photometry Units
Interferometry/ photometry splitter
I(u)
Anamorphic optics
Filters
Polarizers
Dispersive elements
Camera optics
D/λ
Bij/λ
Thermal background
Photometry
Coherent flux
+
Thermal background + photometry for each beam

MATISSE FUNCTIONS

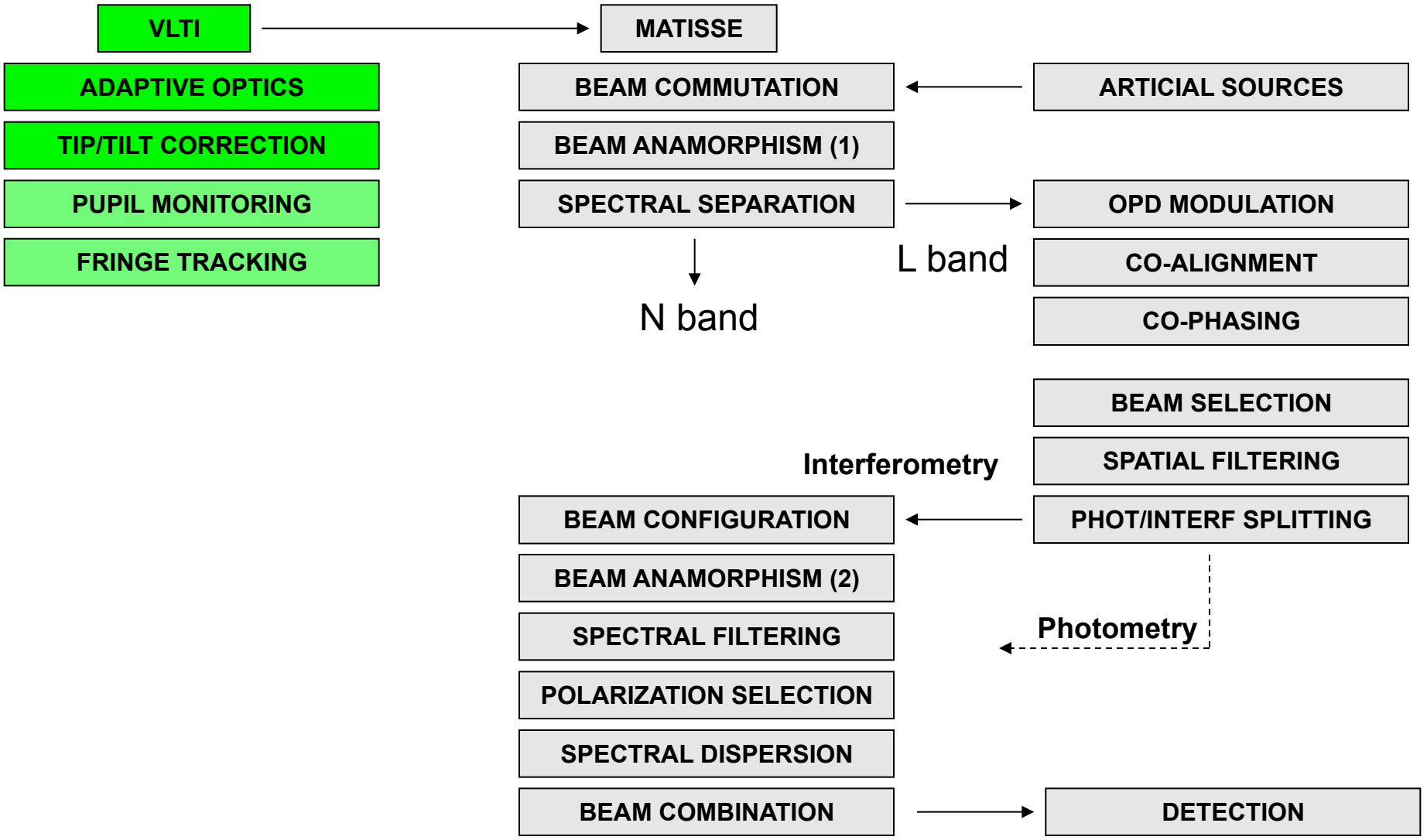

MATISSE FUNCTIONS

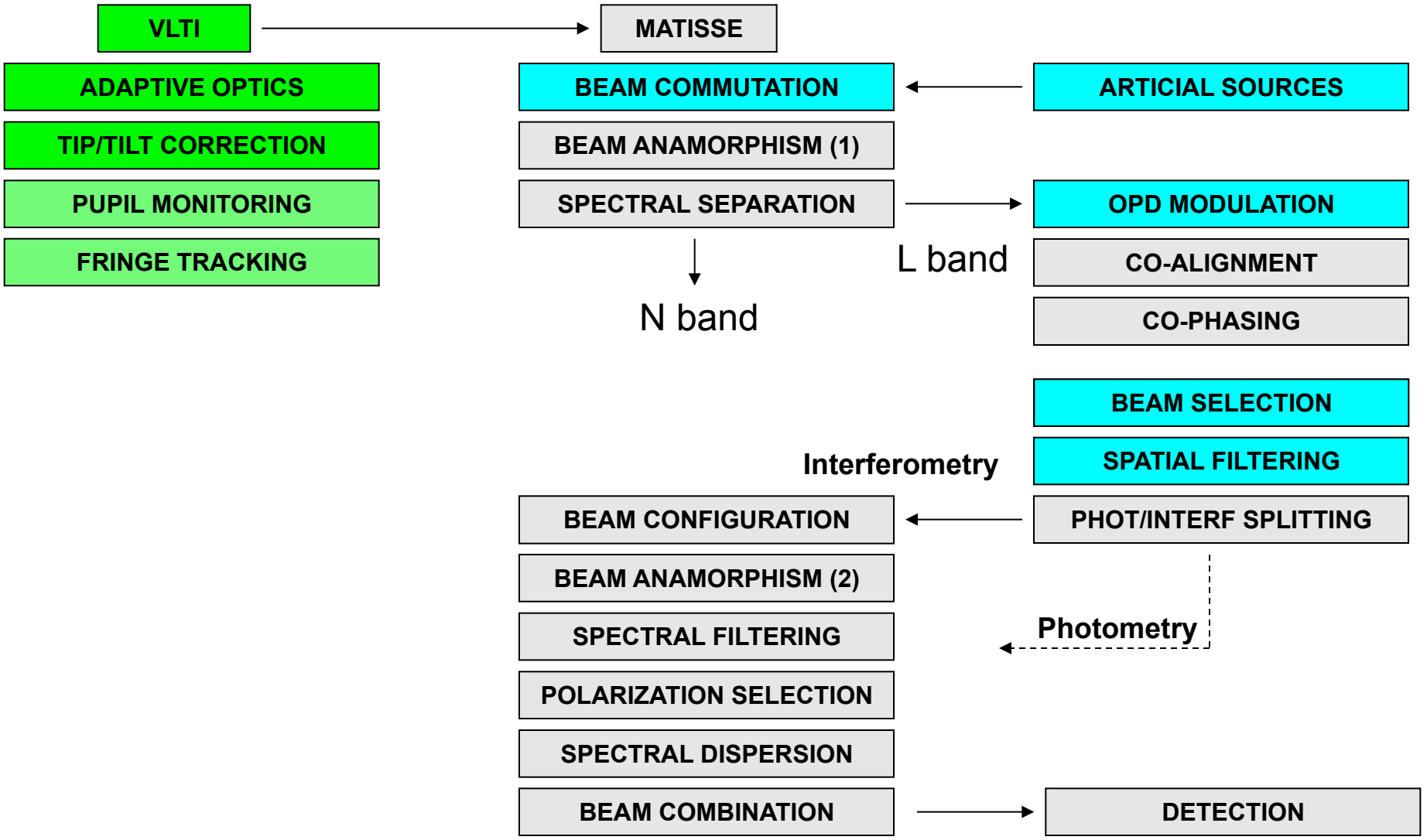

MATISSE FUNCTIONS

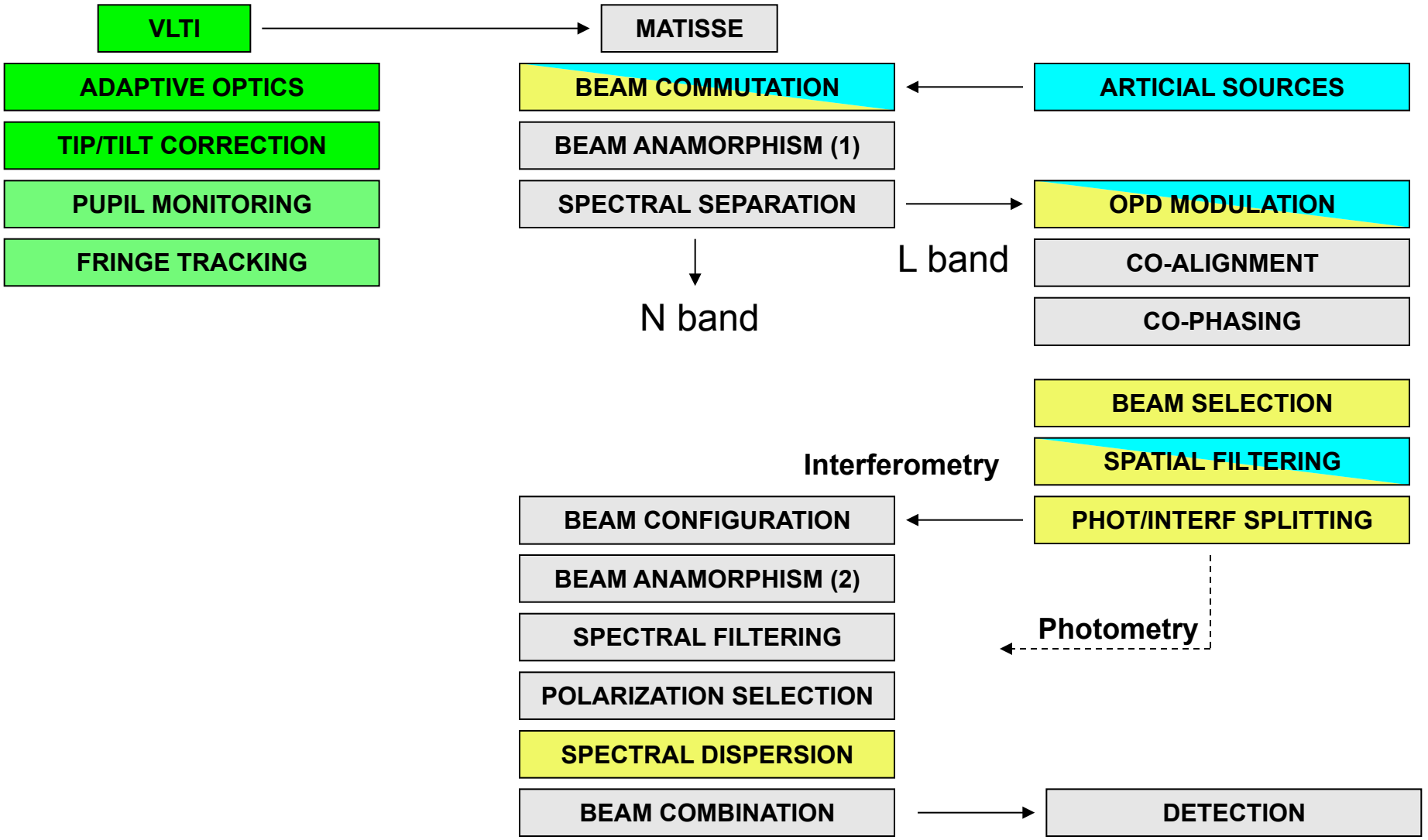

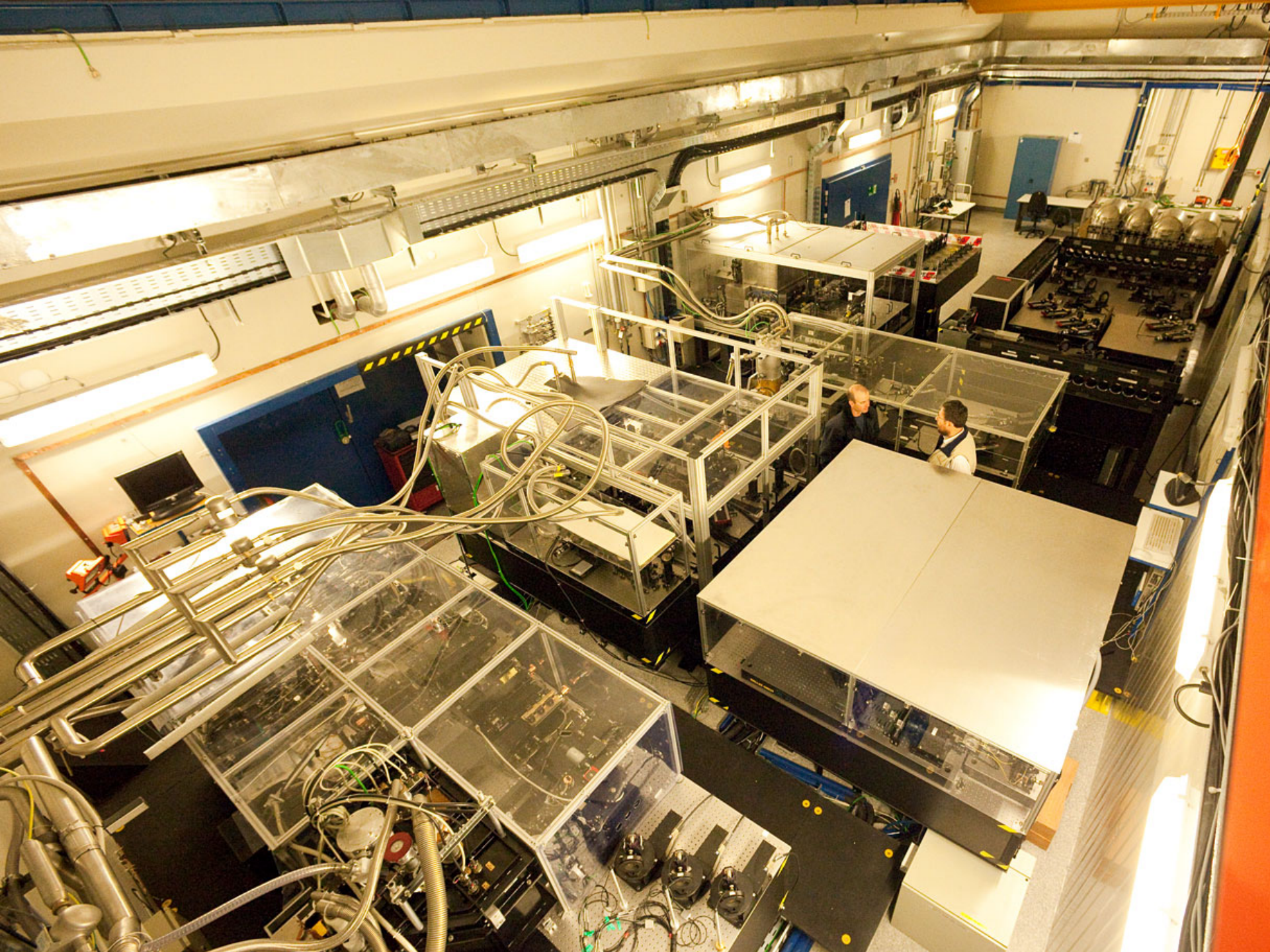

MATISSE in the focal laboratory

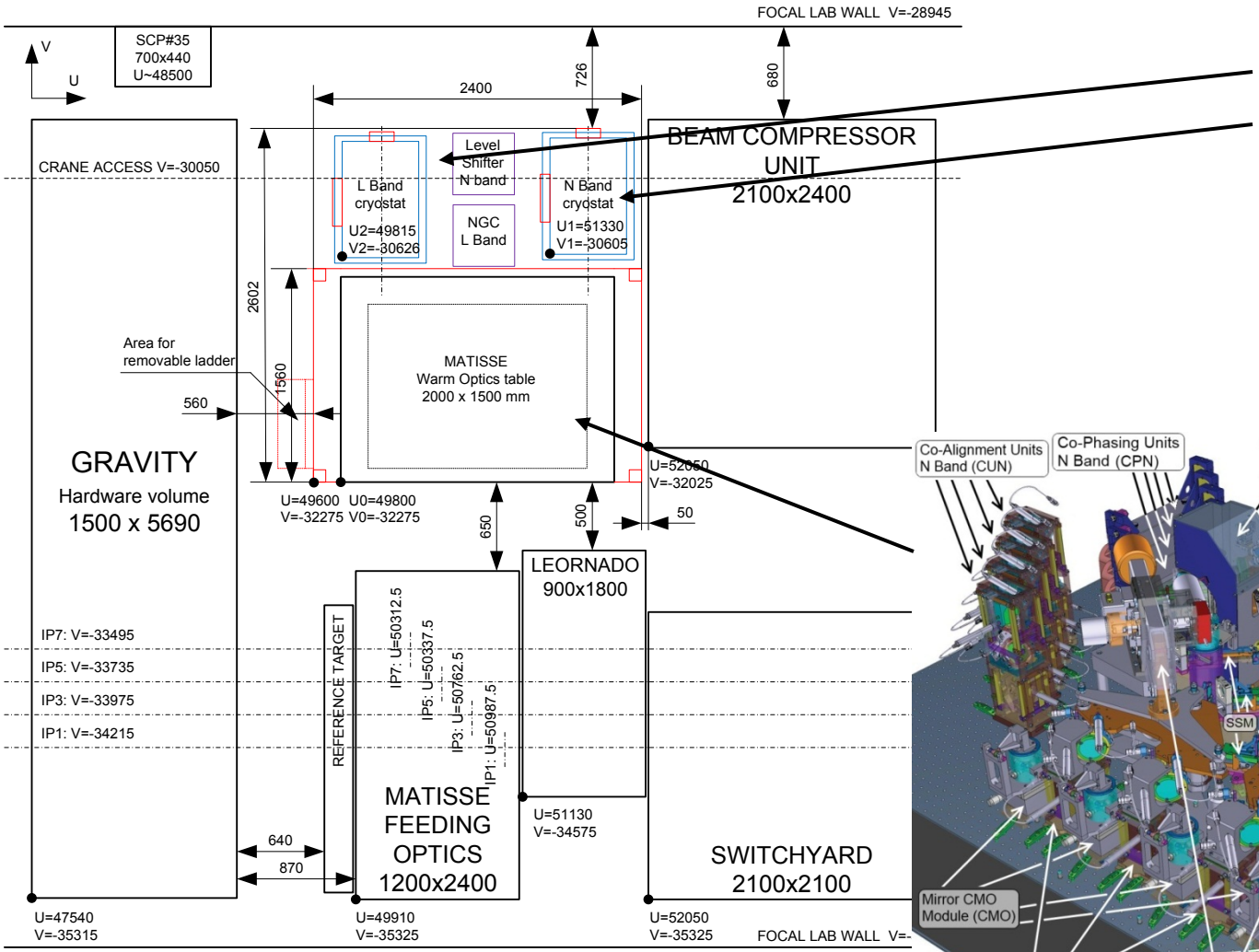

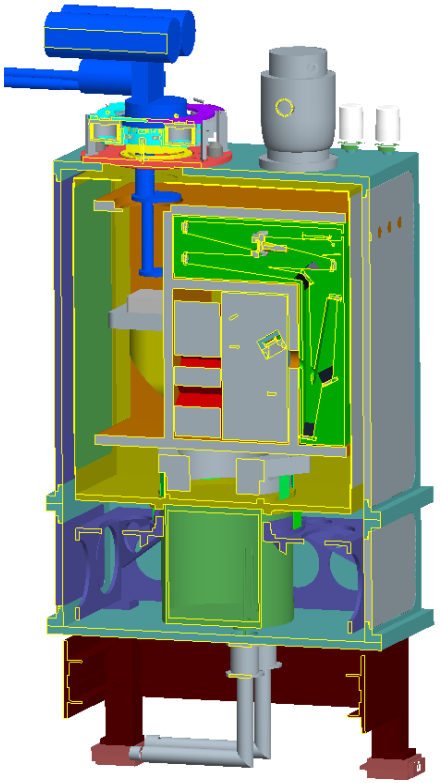

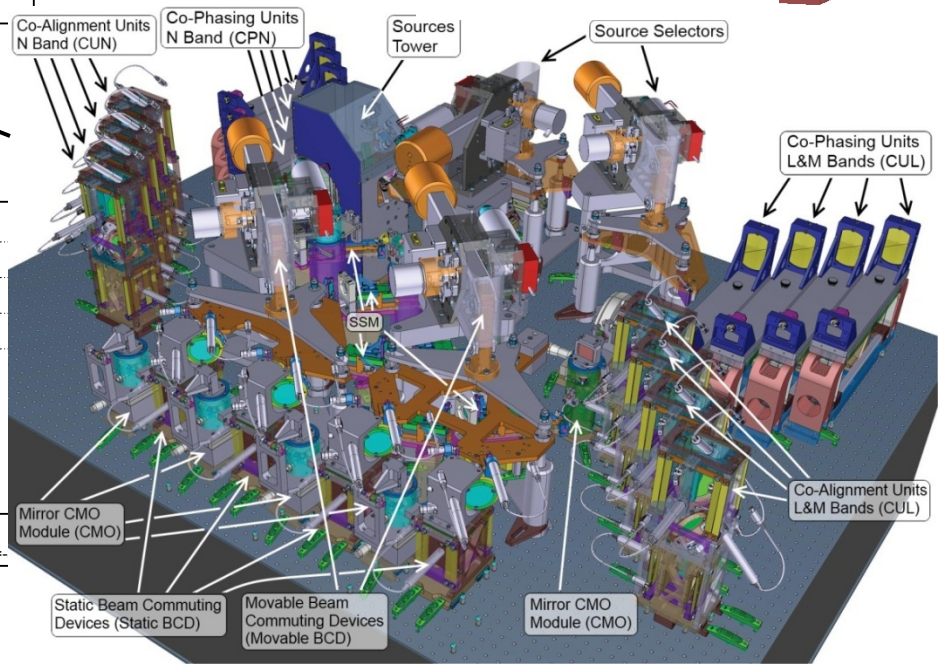

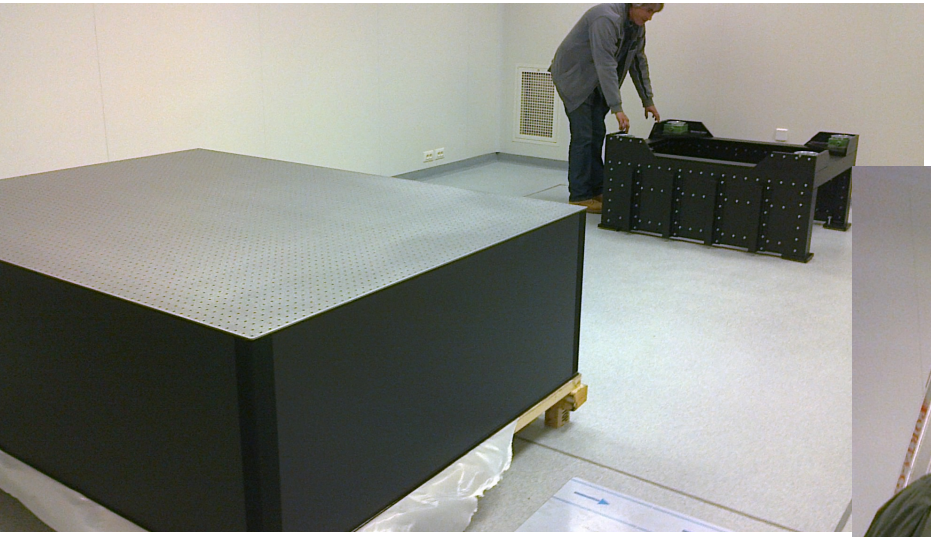

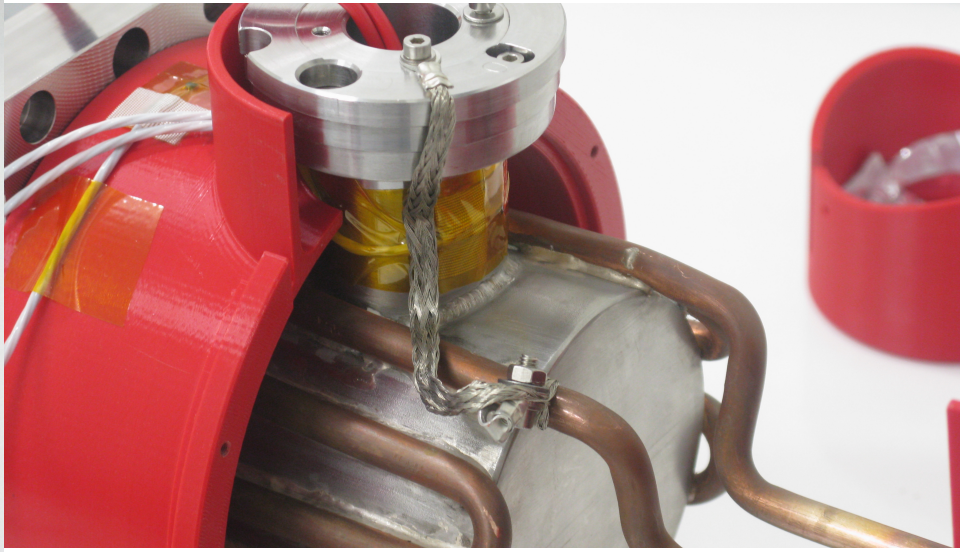

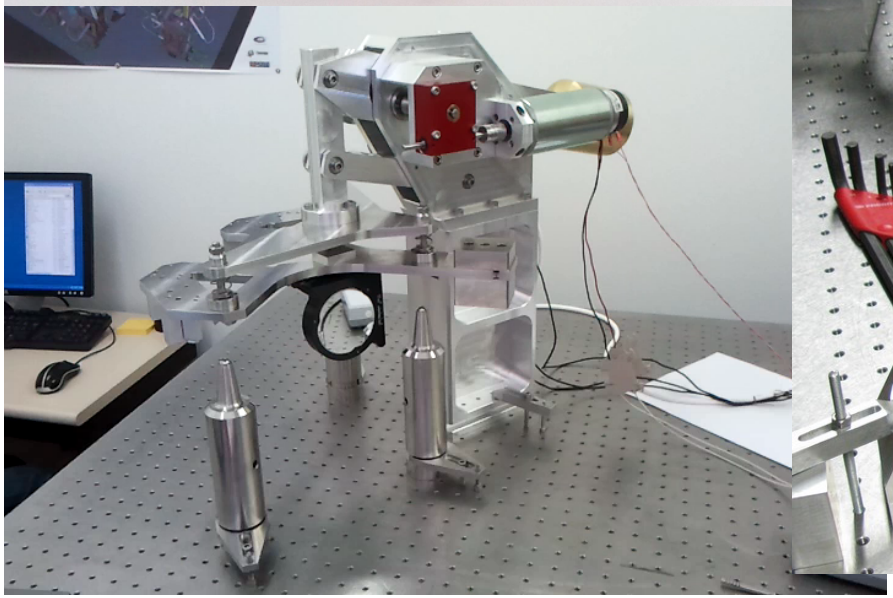

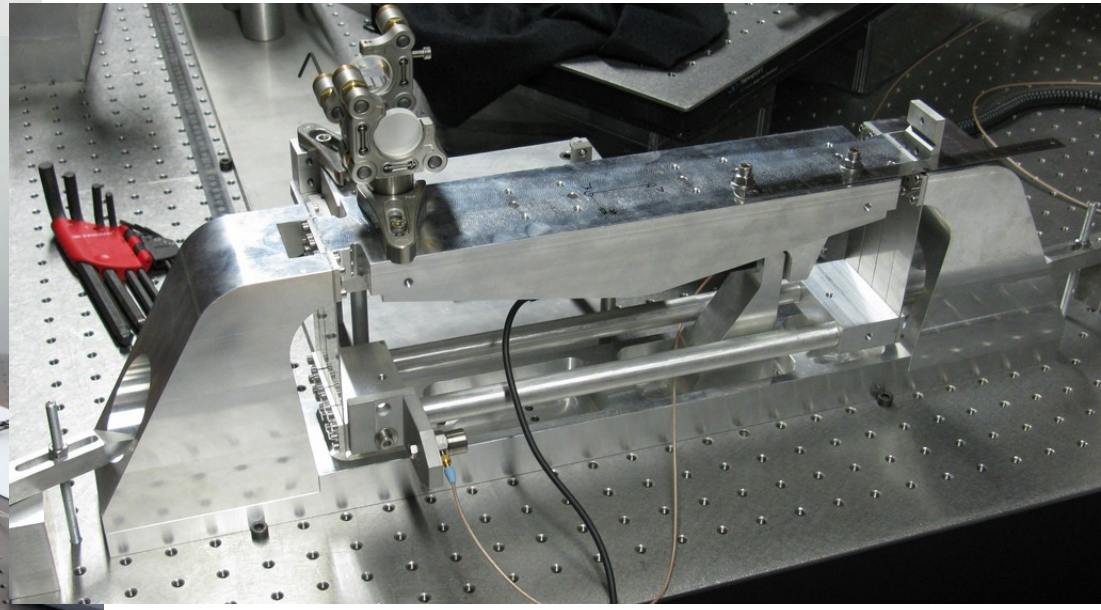

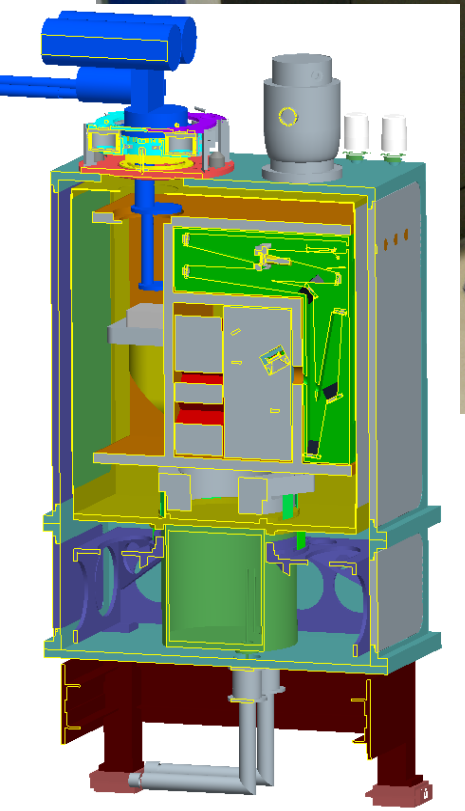

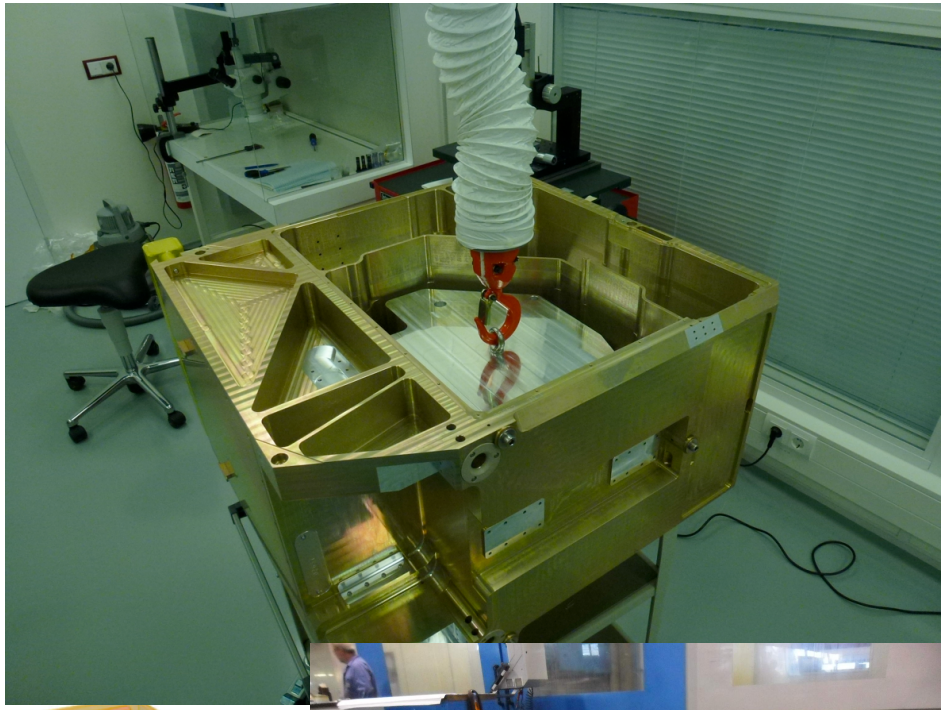

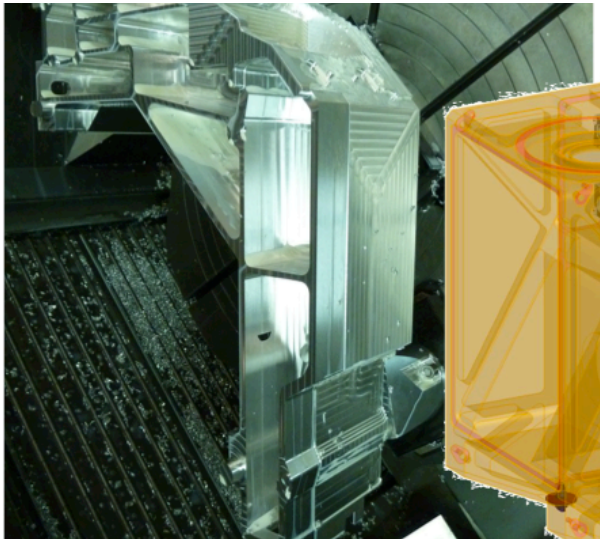

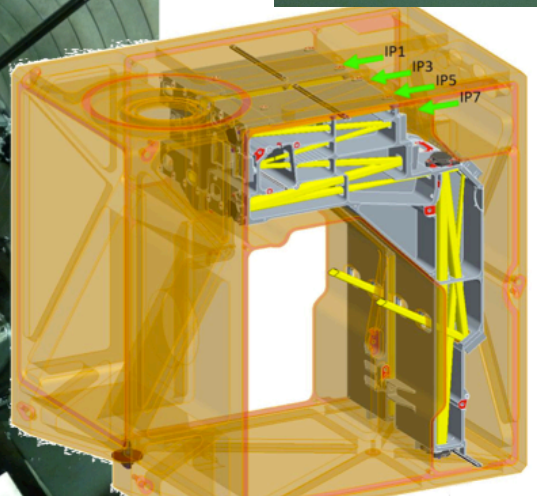
IP1
IP3
IP5
IP7

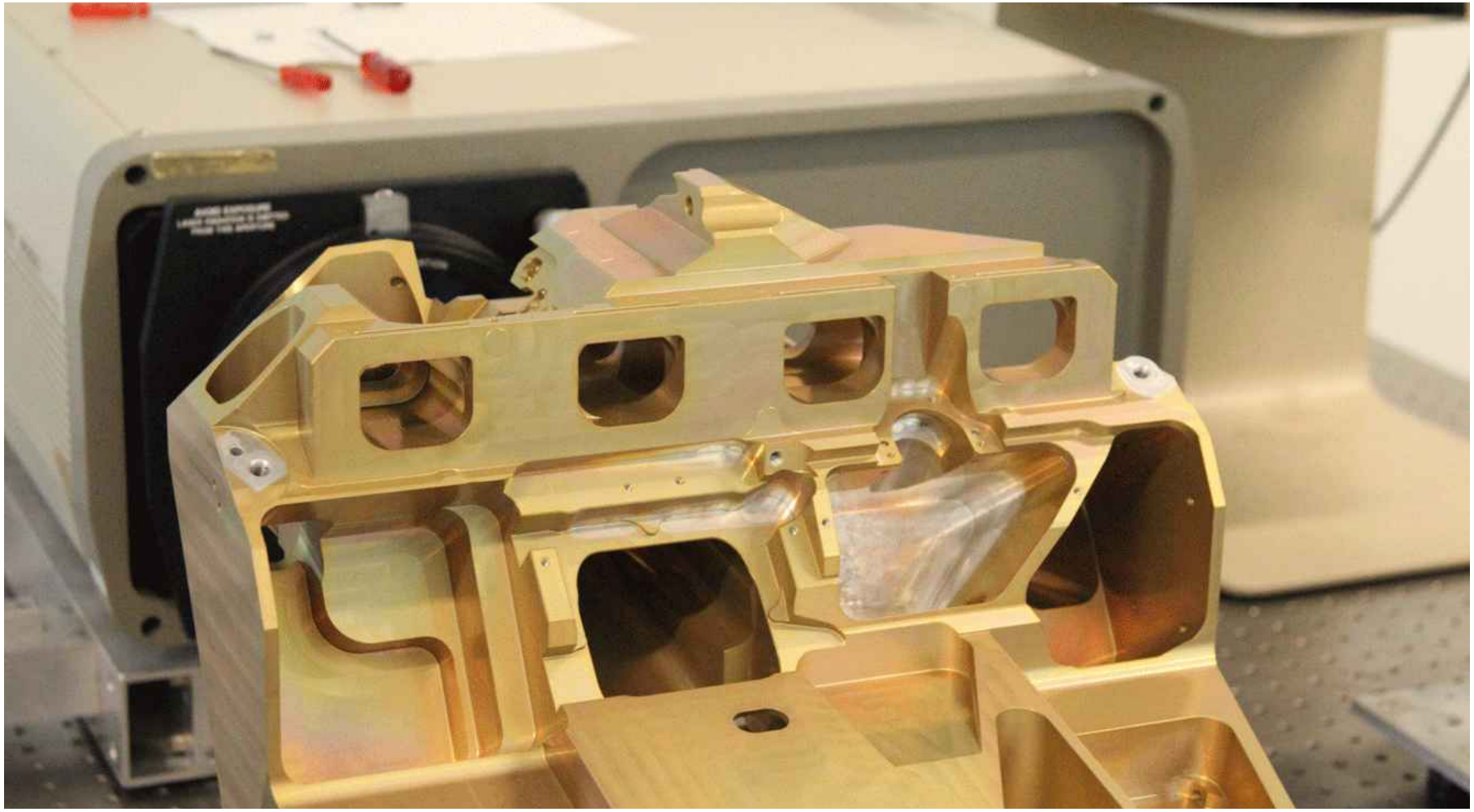

Concept of the instrument

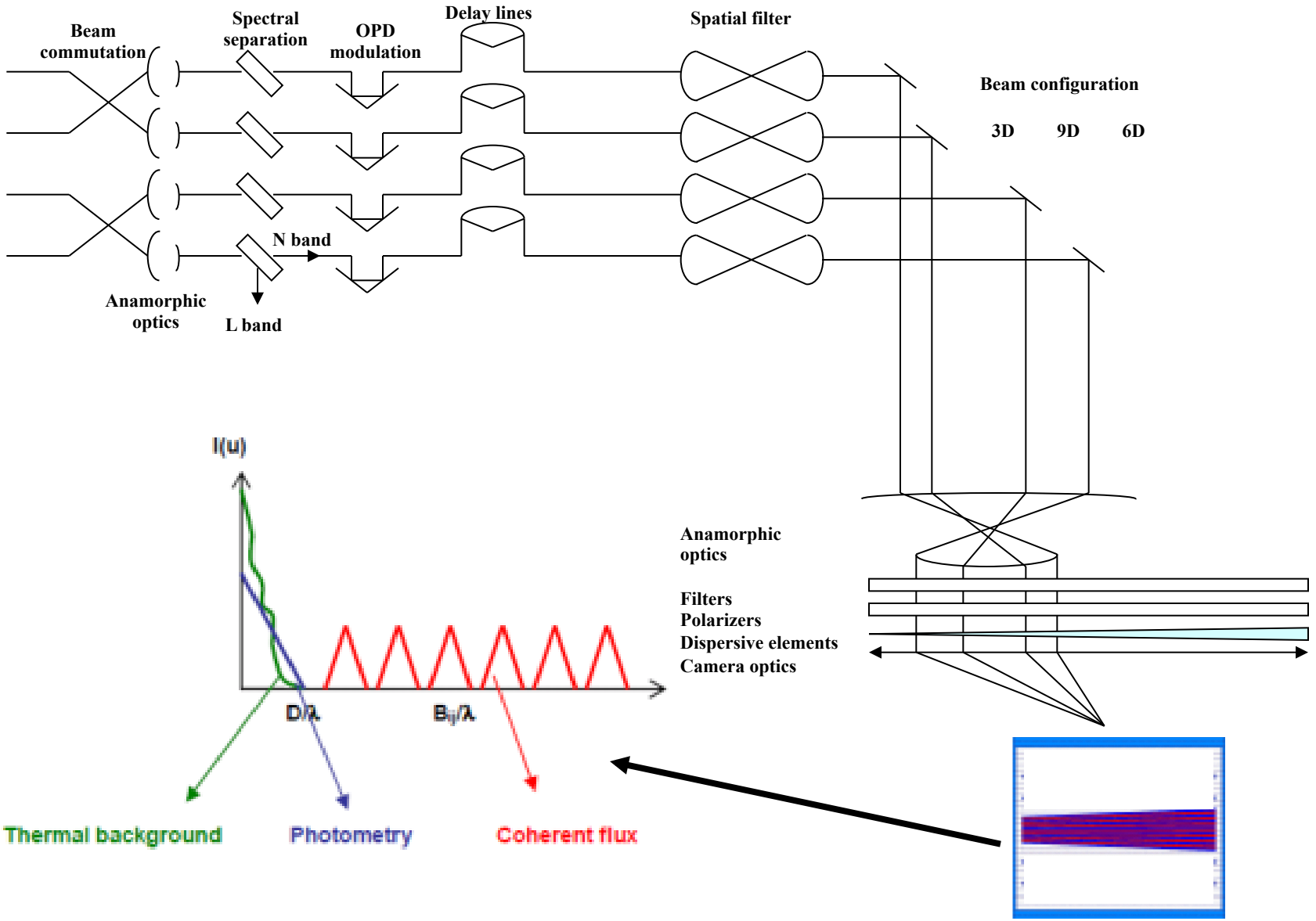

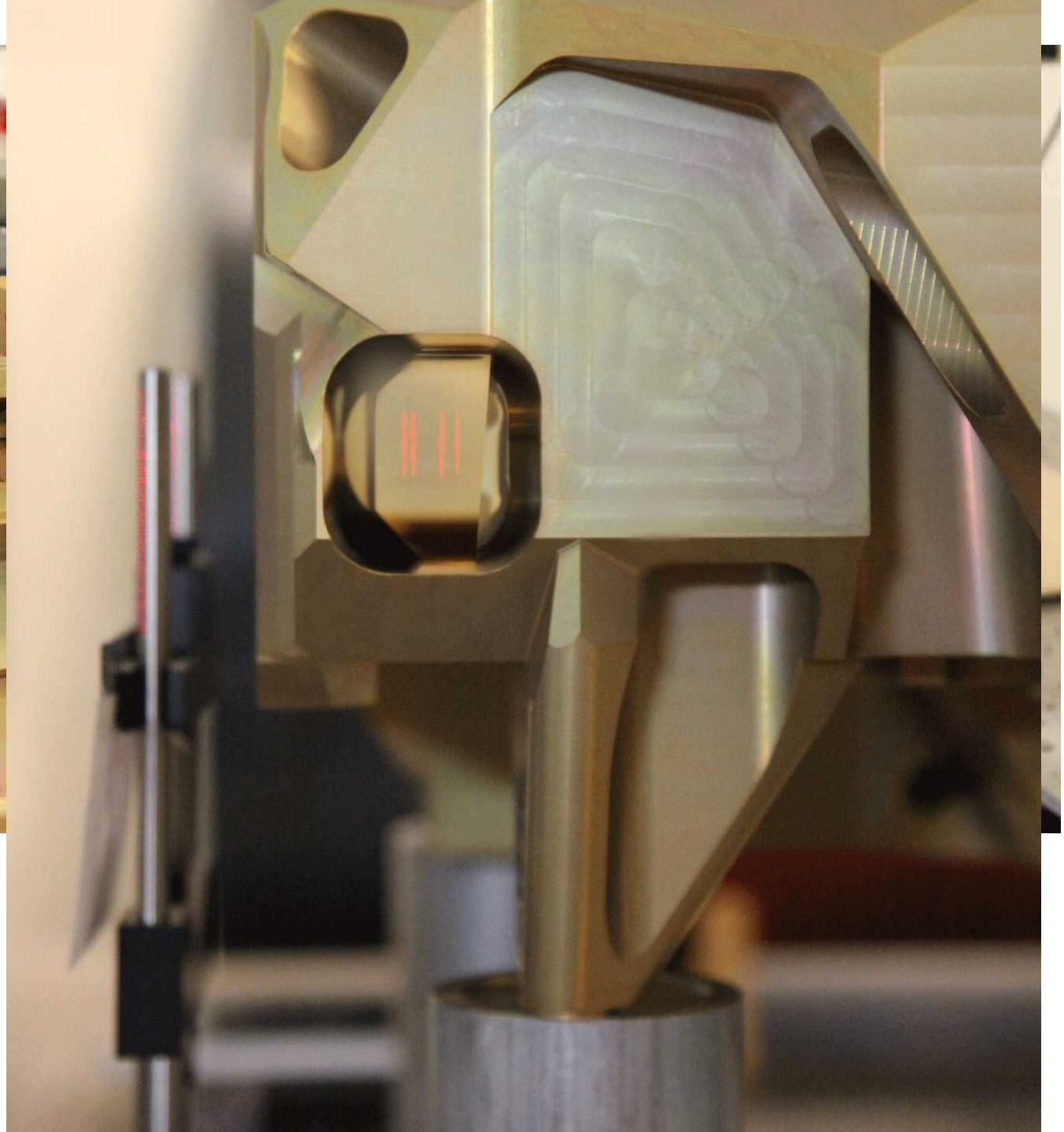

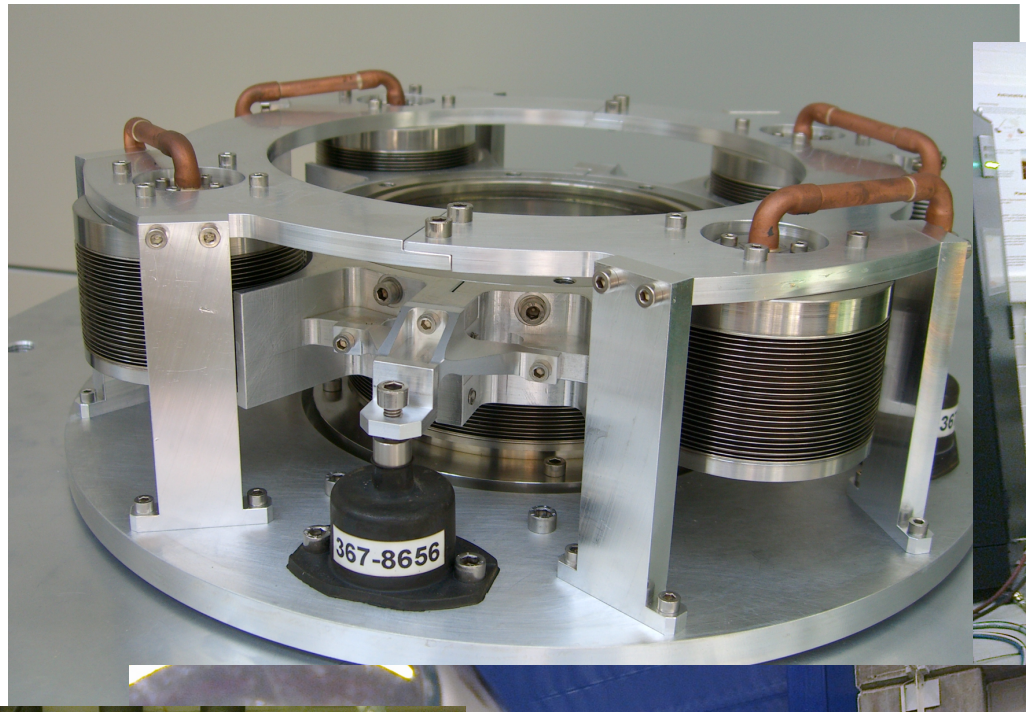
367-8656


HIGH
PRESSURE

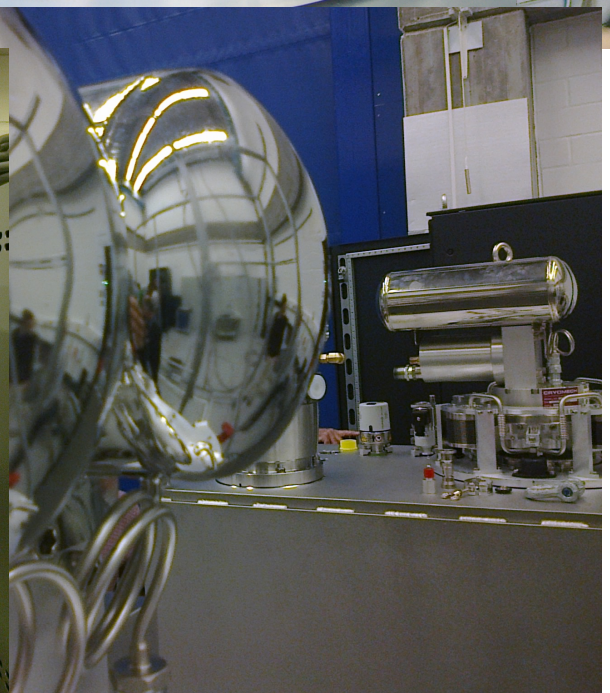

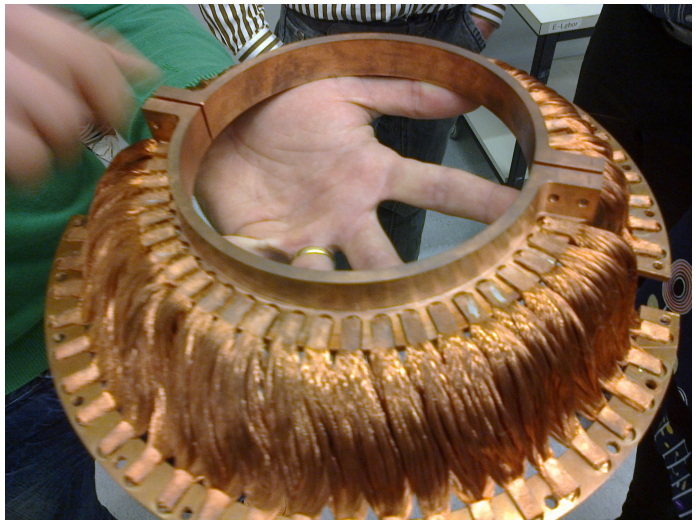

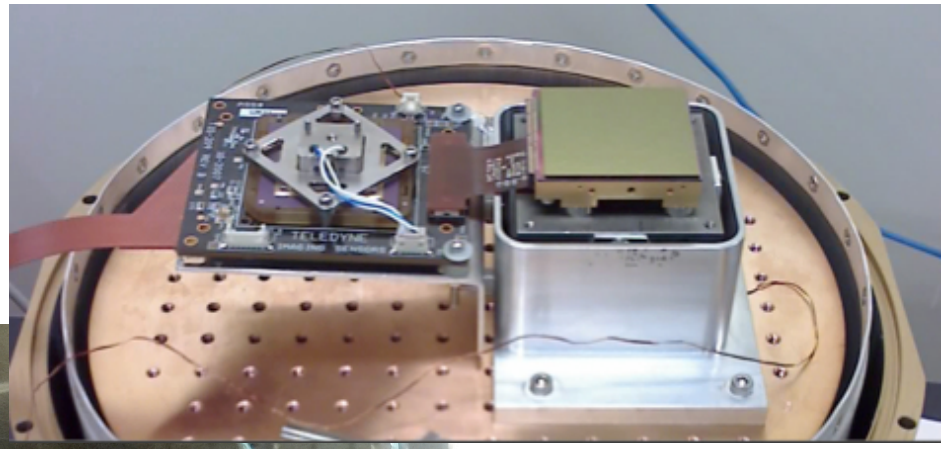
TELEDYNE

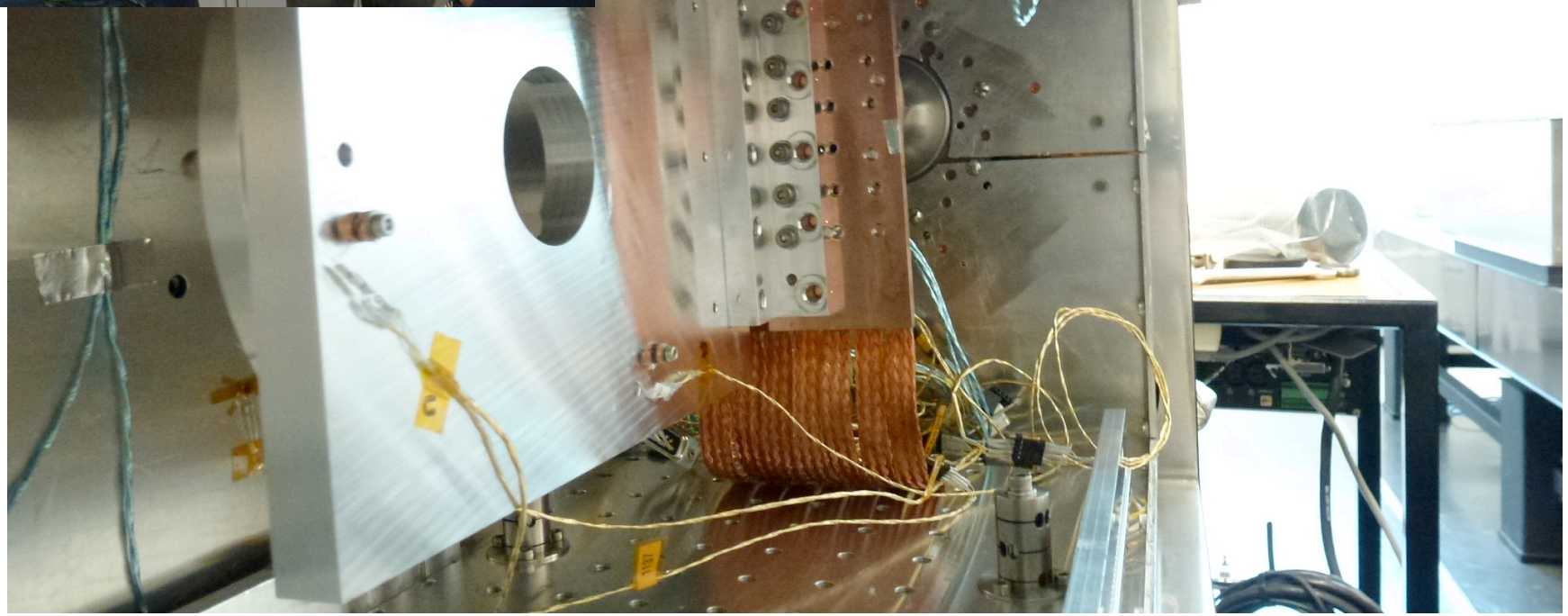

Spectral domain & signatures in the MATISSE domain

Highlights: L& M band ~ 2.9 – 5.0 mm

- Transition from dust scattering to dust emission
- New dust species: e.g., H_2O ice at 3.14 μm
- H_2O gaz broad band feature (2.8 – 4.0 μm)
- H recombination lines, Bra 4.05 μm, Pfb at 4.65 μm
- Polycyclic Aromatic Hydrocarbons (PAHs): 3.3 μm, 3.4 μm
- Nano-diamonds: 3.52 μm
- CO fundamental transition series (4.6 –4.78 μm)
- CO ice features 4.6 – 4.7 μm

N Band ~ 7.5 – 13.5 μm

- Spectral features to be investigated with MATISSE will be similar to those studied with MIDI : Silicates, Olivine, Forsterite, SiC.

Mineralogy and radial transportation in protoplanetary disks

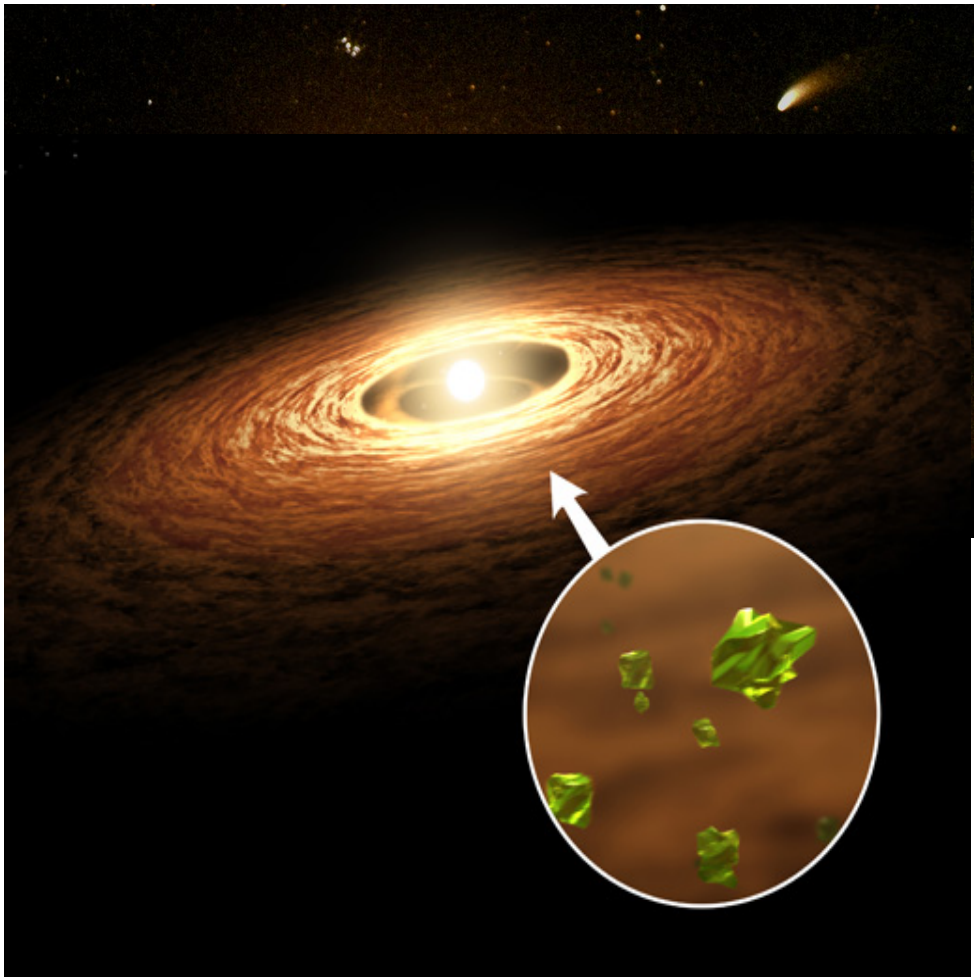

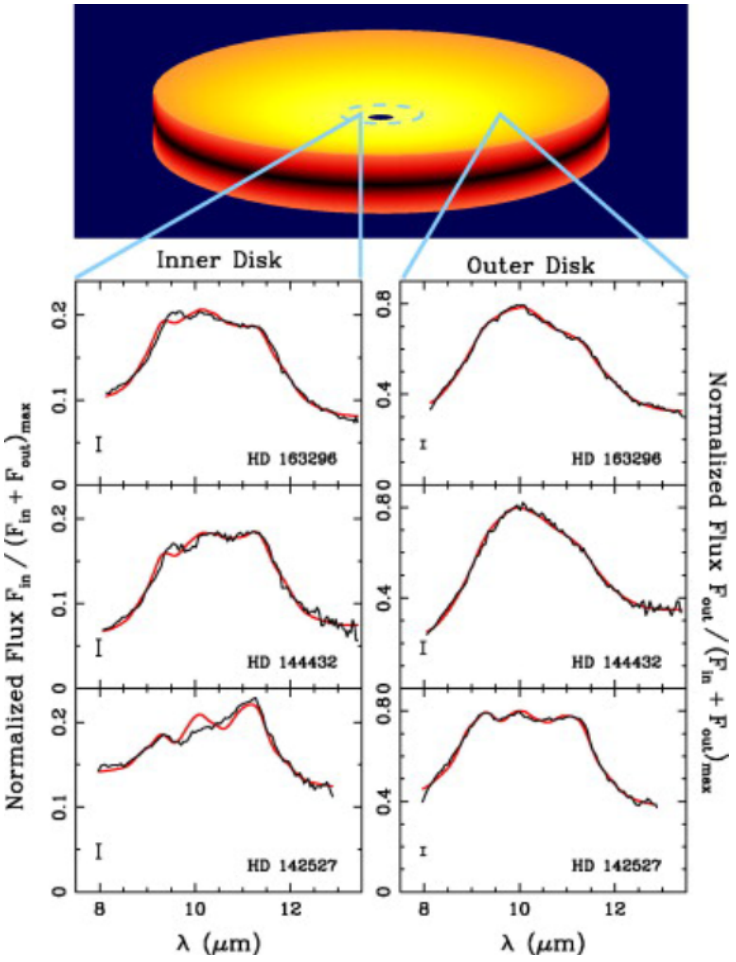

Van Boekle et al. 2004

Example of PAHs and Brα emission

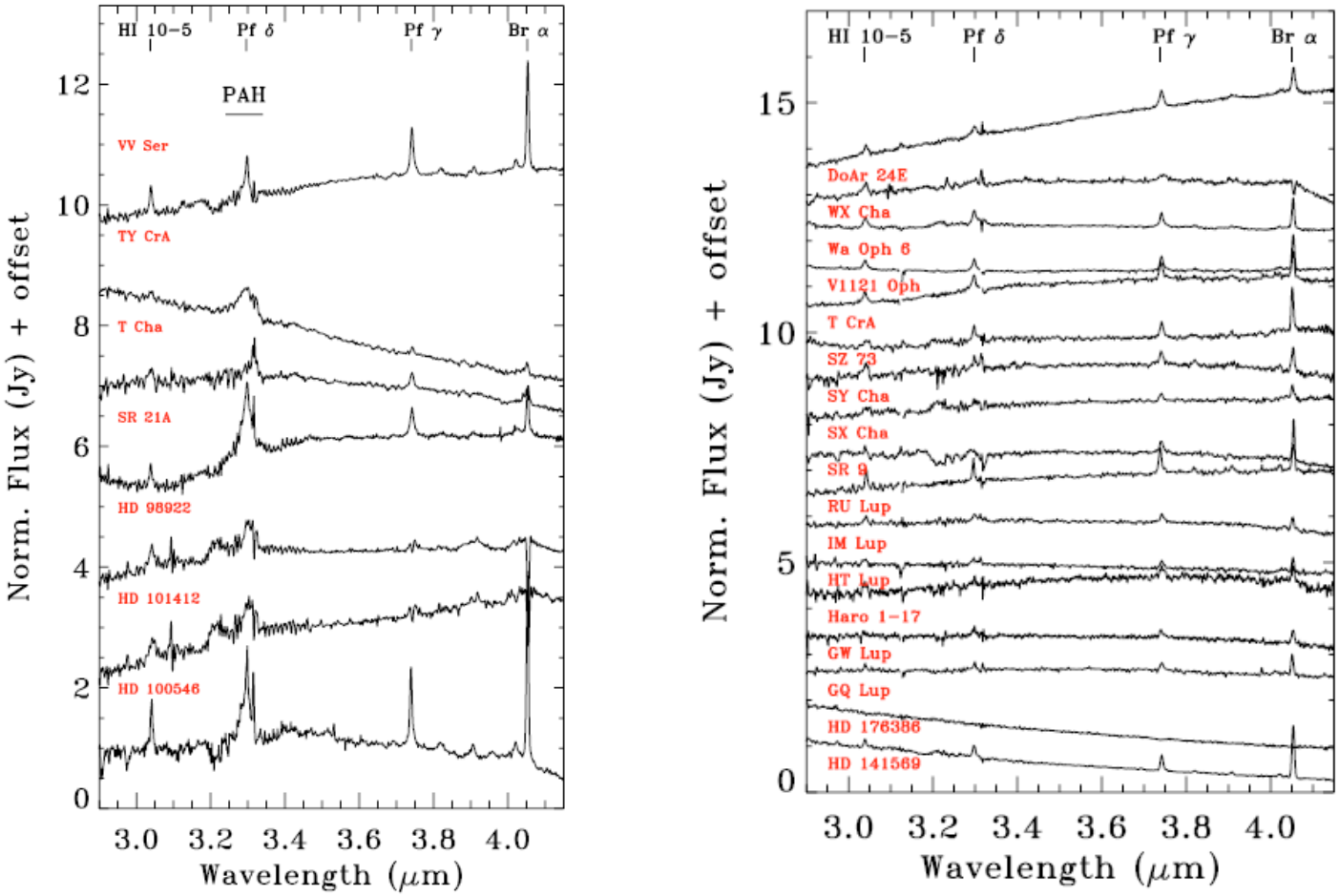

ISAAC L band observations, Geers et al. 2007, A&A 476, 279

Example of CO line(s) emission

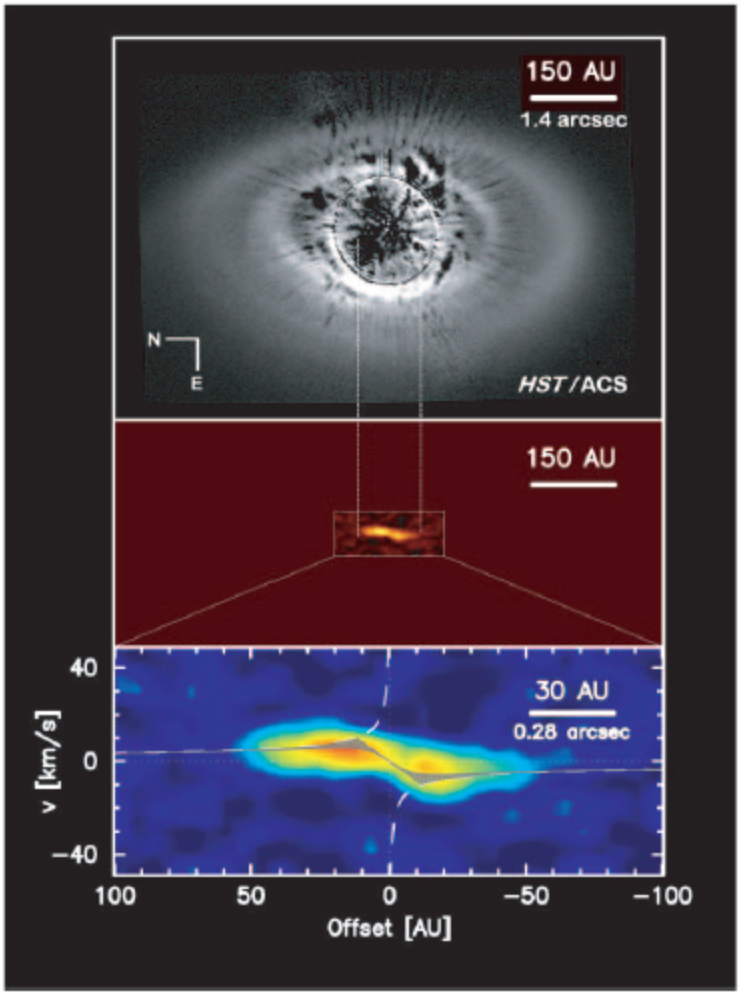

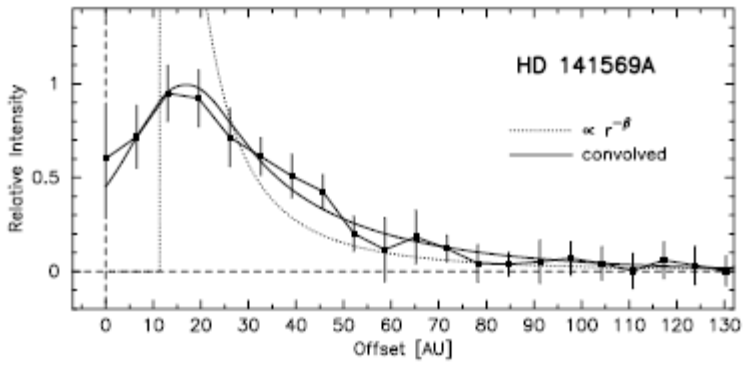

FIG. 2.—Radial profile of CO line emission at the central part of the disk. A power-law radial profile (*dotted line*) was fit to the observation after convolution with the PSF (*solid line*) to find the best-fit cutoff radius at $r_i = 11 \pm 2$ AU. The error bars (1σ) are given by the standard deviation of the radial profiles extracted from CO $v = 2$–1 $R(5)$ to $R(9)$.

GEMINI AO observations, Goto et al. 2006, ApJ 652, 758

Performance

L band (4T SiPhot, Low Resolution)

L band Low resolution		Technical Specifications		Estimated Performances without FT
		Specifications	Goals	
Sensibility	AT	7.5 Jy (L=3.95)	1.5 Jy	2.85 Jy (L=5); (L=6.8 with FT)
	UT	0.75 Jy (L=6.45)	0.15 Jy	0.26 Jy (L=7.6); (L=9.5 with FT)
For a 20 Jy source				
Visibility	AT	≤ 7.5 %	≤ 2.5 %	≤ 1.6 %
	UT	≤ 7.5 %	≤ 2.5 %	≤ 2.3 %
Closure Phase	AT	≤ 80 mrad	-	≤ 20.3 mrad
	UT	≤ 40 mrad	≤ 1 mrad	≤ 20 mrad
Differential Visibility	AT	≤ 3 %	≤ 1 %	≤ 0.7 %
	UT	≤ 1.5 %	≤ 0.5 %	≤ 0.8 %
Differential Phase	AT	≤ 60 mrad	-	≤ 19.3 mrad
	UT	≤ 30 mrad	≤ 1 mrad	≤ 22.2 mrad

Performance

N band (4T SiPhot, Low Resolution)

N band Low resolution		Technical Specifications		Estimated Performances (without FT)
		Specifications	Goals	
Sensibility	AT	60 Jy (N=-0.55)	12.5 Jy	14.6 Jy (N=1)
	UT	4 Jy (N=2.4)	1 Jy	0.9 Jy (N=4)
For a 20 Jy source				
Visibility	AT	≤ 30 %	≤ 10 %	≤ 8.6 %
	UT	≤ 7.5 %	≤ 2.5 %	≤ 2.8 % (≤ 1.2 % with FT)
Closure Phase	AT	≤ 80 mrad	-	≤ 28.2 mrad
	UT	≤ 40 mrad	1 mrad	≤ 13.6 mrad
Differential Visibility	AT	≤ 30 %	≤ 10 %	≤ 8.4 %
	UT	≤ 5 %	≤ 2 %	≤ 1.5 % (≤ 0.8 % with FT)
Differential Phase	AT	≤ 60 mrad	-	≤ 26.1 mrad
	UT	≤ 30 mrad	1 mrad	≤ 24.9 mrad

Basic equations

Sky + Object

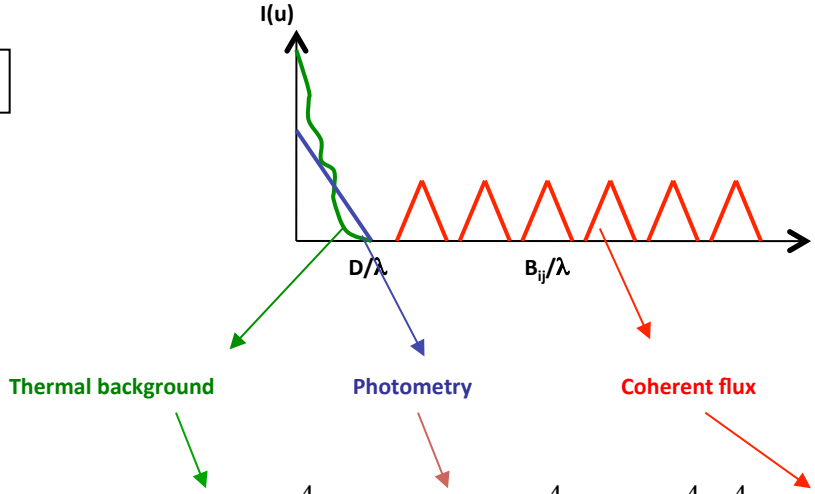

Interferogram: $$I(u) = M_b(u).\sum_{i=1}^{4} n^I{}_{bi} + M(u).\sum_{i=1}^{4} n^I{}_i + \sum_{i=1}^{4}\sum_{\substack{j=2 \\ j>i}}^{4} M(u-u_{ij}).\sqrt{n^I{}_i.n^I{}_j}\,V_{ij}$$

Photometry: $$P_i(u) = [M_b(u).n^P{}_{bi} + M(u).n^P{}_i]$$

Sky only

« Interferogram »: $$I_S(u) = M_b(u).\sum_{i=1}^{4} n^I{}_{bi}$$

Photometry: $$S_i(u) = M_b(u).n^P{}_{bi}$$

SNR on coherent flux

- OPD modulation
- Multi-axial configuration

⇒ Elimination of the thermal background

However residual contamination of the thermal background on fringe peak (windowing effect)

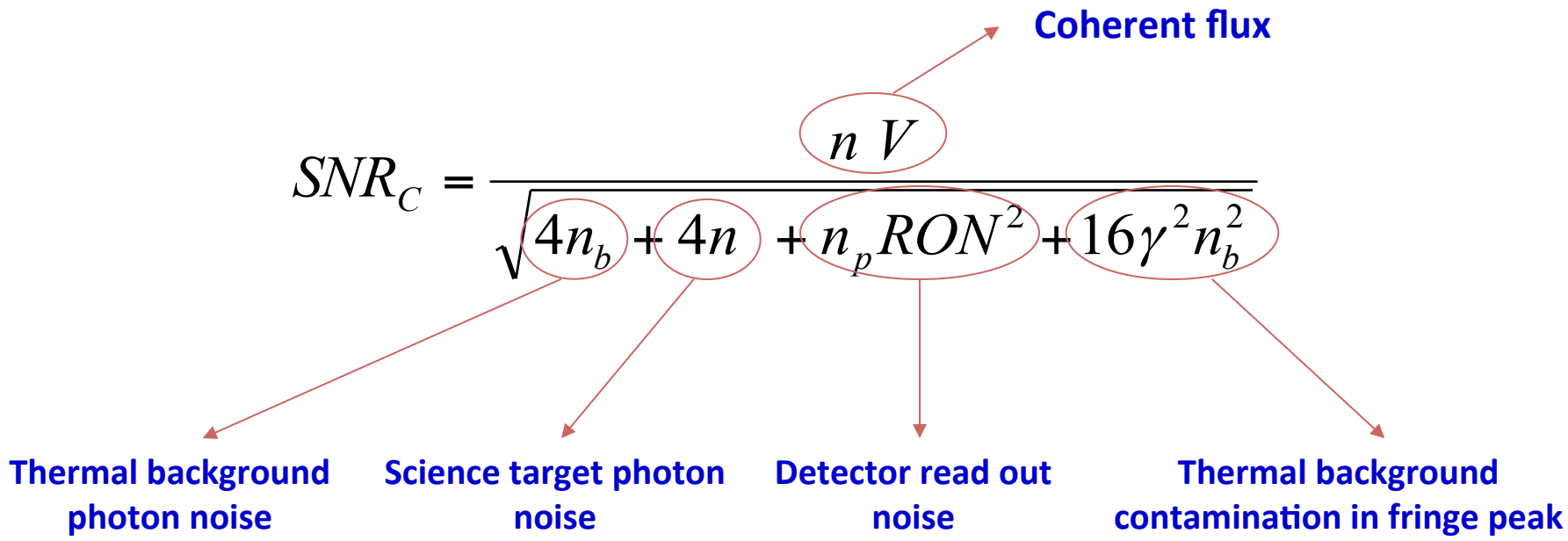

SNR on photometry

➢ **Chopping: Photometry estimation: OBS(Target+Sky) – OBS(Sky)**

⇒ **Elimination of the thermal background**

However residual contamination of the thermal background (variation between obs)

Photometry

$$SNR_n = \frac{n^p}{\sqrt{2n_b^p + n^p + n_p^{'} RON^2 + D_B\left(1/f_{chop}\right)}}$$

Thermal background photon noise

Science target photon noise

Detector read out noise

Thermal background variation between obs

SNR on visibility and phases

Visibility:

$$SNR_V = \frac{1}{\sqrt{\frac{1}{SNR_C^2} + \frac{1}{SNR_n^2}}}$$

Closure phase:

$$\sigma_\psi^2 \approx \frac{3}{2}\left(\frac{1}{SNR_C^2}\right)$$

Differential phase:

$$\sigma_\phi^2 \approx \frac{1}{2}\left(\frac{1}{SNR_C^2}\right)$$

Sensitivity: **Limiting magnitude $SNR_C = 3$ in the coherence time (pessimistic → coherent processing)**

SNR calculation

Photons from science target n:

- Brightness of the source, spectral bandwidth, telescope surface, …
- Transmission of the atmosphere, of the VLTI, of MATISSE
- Flux loss due to the spatial filtering
- Flux loss due to the tip/tilt of the beams before the SF
- Flux loss due to the non perfect WFE of the beams
- Flux loss due to the pupil motion
- Detector Quantum efficiency
- ….

Instrumental visibility V:

- Contrast loss due to the imperfect overlap of the beams
- Contrast loss due to the non perfect WFE of the beams
- Contrast loss due to the pupil motion
- Contrast loss due to the OPD jitter
- Contrast loss due to the OPD non equalization
- Contrast loss due to the detection vibration
- Contrast loss due to the polarization effects
- Contrast loss due to the detector pixel crosstalk
- ….

Photons from the thermal background n_b and its variation D, γ:

- Temperatures of the optics
- Transmission of the atmosphere, of the VLTI, of MATISSE
- Field of view
- Spectral bandwidth, telescope surface, …
- Structure function (temporal variation of the thermal background
- Contamination of the thermal background due to the windowing …
- ….

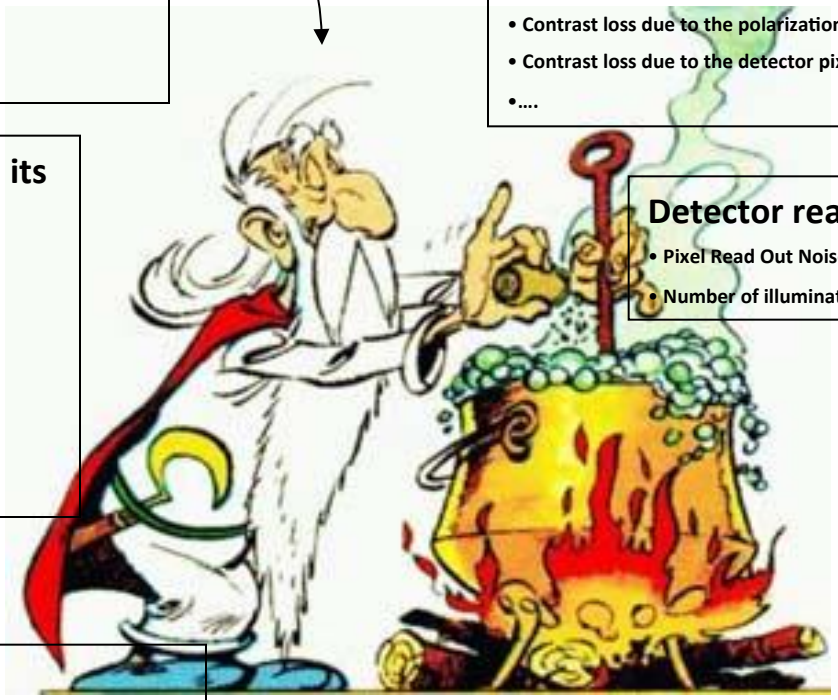

Detector read out noise RON:

- Pixel Read Out Noise
- Number of illuminated pixels

Fundamental Noise

+ Variation between target and calibrator (OPD jitter Strehl ratio Image overlap Pupil jitter

Errors on the calibrated data

Persons and Institutes

B. Lopez[1], P. Antonelli[1], W. Jaffe[3], R. Petrov[1], S. Lagarde[1], L. Venema[4], F. Bettonvil[4], P. Berio[1], R. Navarro[4], U. Graser[2], U. Beckman[5], G. Weigelt[5] , F. Vakili[1], T. Henning[2], S. Robbe-Dubois[1], S. Wolf[6], C. Bailet[1], J. Behrend[5], Y. Bresson[1], O. Chesneau[1], J.M. Clausse[1], C. Connot[5], M. Dugué[1], Y. Fantei[1], E. Elswijk[4], H. Hanenburg[4], K.H. Hofmann[5], M. Heininger[5], R. ter Horst[4], J. Hron[7], J. Kragt[4], N. Tromp[4], T. Agocs[4], G. Kroes[4], W. Laun[2], Ch. Leinert[2], M. Lehmitz, A. Matter[5], A. Meilland[5], J.L. Menut[5], F. Millour[1], U. Neumann*, E. Nussbaum[5], S. Ottogalli[1], J.-U. Pott[2], T. Ratzka, F. Rigal[4], A. Roussel[1], D. Schertl[5], M. Vannier[1], K. Wagner[2], M. Mellein[2], T. Kroener[2], N. Mauclert[1,] Paul Girard[1], G. M. Lagarde[1].

With the involvement at ESO[8] side of : A. Glindemann, J.-C. Gonzales, T. Phan Duc, G. Finger, D. Ives, G. Jakob, I. Percheron, G. Avila, R. Palsa, E. Pozna, J.L. Lizon, Ch. Lucuix, S. Menardi, P. Haguenhauer P., P. Gitton, S. Morel, F. Gonté, P. Jolley, G. Rupprecht, P. Bourget, F. Delplancke, L. Mehrgan, J. Stegmeier and previously at ESO : G. van Belle, A. Richichi, A. Moorwood

1- UMR Lagrange 7239, UNS, CNRS, OCA, BP 4229 06304, Nice Cedex 4 France

2- Max Planck Institute for Astronomy, Germany, 69117, Heidelberg

3- Huygens Laboratory, J.H. Ooort Building, Niels Bohrweg 2, NL-2333 CA Leiden, The Netherlands

4- NOVA Optical- Infrared Instrumentation Group at ASTRON, Postbus 2, 7990 AA, Dwingeloo, The Netherlands

5- Max Planck Institute for Radioastronomy, Germany, 53121 Bonn

6- ITAP, Kiel University, Germany,

7- Institute of Astronomy, University of Vienna , Austria, A-1180, Vienna

8- ESO European Southern Observatory, Karl-Schwarzschild-Str. 2 Germany

* no adds wished

Also Institutes or individual collaborations of : L. Labadie & Khôl University, L. Mosoni & Konkoly Observatory, J.-C. Augereau, W.C. Danchi, T. Ratzka, E. Thiebaut, K. Meisenheimer, R. Lepool, M. Hogerheijde, J.-U. Pott, B. Stecklum, K. Demyk, Ph. Mathias.